Scientific Online

OPEN JOURNAL OF ATMOSPHERIC AND CLIMATE CHANGE
ISSN(Print): 2374-3794 ISSN(Online): 2374-3808
DOI: 10.15764/ACC.2014.03001
Volume 1, Number 3, November 2014

OPEN JOURNAL OF ATMOSPHERIC AND CLIMATE CHANGE

Advanced Two-Layer Climate Model for the Assessment of Global Warming by CO_2

Hermann Harde*

Experimental Physics and Materials Science, Helmut-Schmidt-University, Hamburg, Germany.
***Corresponding author**: harde@hsu-hh.de

Abstract:
We present an advanced two-layer climate model, especially appropriate to calculate the influence of an increasing CO_2-concentration and a varying solar activity on global warming. The model describes the atmosphere and the ground as two layers acting simultaneously as absorbers and Planck radiators, and it includes additional heat transfer between these layers due to convection and evaporation. The model considers all relevant feedback processes caused by changes of water vapour, lapse-rate, surface albedo or convection and evaporation. In particular, the influence of clouds with a thermally or solar induced feedback is investigated in some detail. The short- and long-wave absorptivities of the most important greenhouse gases water vapour, carbon dioxide, methane and ozone are derived from line-by-line calculations based on the HITRAN08-databasis and are integrated in the model. Simulations including an increased solar activity over the last century give a CO_2 initiated warming of *0.2 ˚C* and a solar influence of *0.54 ˚C* over this period, corresponding to a CO_2 climate sensitivity of *0.6 ˚C* (doubling of CO_2) and a solar sensitivity of *0.5 ˚C* (*0.1 %* increase of the solar constant).

Keywords:
Carbon Dioxide; Climate Model; Climate Sensitivity; Cloud Cover; Global Warming; Solar Activity

1. INTRODUCTION

Understanding of recent changes in the climate system results from combining observations, studies of feedback processes, and model simulations [1]. Although the substantiated state of knowledge about the Earth-atmosphere system (*EASy*) could significantly be improved over the last decade, explanations of the observed global warming over the last century are quite manifold and contradictory. One reason might be that quite different and even counteracting processes control our climate, and it is not always clear what individual contribution they have. The weighting of these processes in model simulations have significant consequences on the implications what really determines our future climate.

Many climate models, particularly the Atmosphere-Ocean General Circulation Models (*AOGCMs*) [2] were developed not only to simulate the global scenario, but also to predict local climate variations and this as a function of time. Therefore, they have to solve a dense grid of coupled nonlinear differential equations depending on endless additional parameters, which make these calculations extremely time consuming and even instable. So, smallest variations in the initial constraints or corrections on a multidimensional

parameter platform already cause large deviations in the final result and can dissemble good agreement with some observations but with completely wrong conclusions.

For the actual assessment of one of the most fundamental quantities in climate sciences, the *equilibrium climate sensitivity*, representing the temperature increase at doubled CO_2 concentration [2], *p*.629, the *Intergovernmental Panel on Climate Change* (*IPCC*) favours the concept of radiative forcing (*RF*), which is supposed to be appropriate to describe the transition of the surface-troposphere system from one equilibrium state to another in response to an externally imposed perturbation. However, generally this concept only describes a *1st* order approximation on such external perturbation [3], *p*.354. So, it is assumed that with increasing greenhouse (*GH*) gas concentration additionally absorbed radiation in a first step only causes a temperature increase of the atmosphere up to a level, at which the atmosphere just can release the additional absorption as increased radiation energy to space. A feedback to the Earth's surface is then supposed as linear response to the perturbation, where the increased atmospheric temperature is simply transposed one to one to the surface without considering significant interrelations between both layers, generally causing a completely new radiation and energy balance after the perturbation. So, convection and evaporation processes are directly temperature dependent, and any radiation flux varies strongly nonlinear with the *4th* power to the temperature. All this modifies the amount of re-absorbed radiation in the atmosphere and the direct radiation losses to space. Thus, the response of *EASy* on any perturbation cannot be deduced from the temperature response of the atmosphere alone, but has to satisfy the energy balance at the surface as well as at the top of the atmosphere (*TOA*), which results in a new thermal equilibrium of *EASy*.

In contrast to the *RF*-concept and the extremely complex *AOGCMs* here we present an advanced two-layer climate model, especially appropriate to calculate the influence of increasing CO_2 concentrations on global warming as well as the impact of solar variations on the climate. The model describes the atmosphere and the ground as two layers acting simultaneously as absorbers and Planck radiators, and it includes additional heat transfer between these layers due to convection and evaporation. At equilibrium both, the atmosphere as well as the ground, release as much power as they suck up from the sun and the neighbouring layer. An external perturbation, *e.g.*, caused by variations of the solar activity or the *GH*-gases then forces the system to come to a new equilibrium with new temperature distributions for the Earth and the atmosphere.

The model includes short- (*sw*) and long-wave (*lw*) scattering processes at the atmosphere and at clouds, in particular it considers multiple scattering and reflection between the surface and clouds. It also includes the common feedback processes like water vapour, lapse rate and albedo feedback, but additionally takes into account temperature dependent sensible and latent heat fluxes as well as a temperature induced and solar induced cloud cover feedback.

While propagation losses of radiation in the atmosphere are generally expressed by a radiative forcing term, we trace any changes of *GH*-gas concentrations back to the *sw* and *lw* absorptivities of these gases, which therefore, represent the key parameters in our climate model. These absorptivities are calculated for the most important *GH*-gases water vapor, carbon dioxide, methane and ozone and are derived from line-by-line calculations based on the HITRAN08-database [4]. Since the concentration of the *GH*-gases and the atmospheric pressure are changing with temperature and altitude, these calculations are performed for up to 228 sub-layers from ground to *86 km* height and additionally for three climate zones, the tropics, mid-latitudes and high-latitudes. Finally, to determine, how these absorptivities change with the CO_2 concentration, all these calculations, for the sub-layers and climate zones, are repeated for 14 different concentrations from *0-770 ppm* at otherwise same conditions.

The changing path length of sun light in the sub-layers, which depends on the angle of incidence to the atmosphere and, therefore, on the geographic latitude and longitude, is included by considering the Earth as a truncated icosahedron (Bucky ball) consisting of 32 surface elements with well defined angles to the incident radiation, and then assigning each of these areas to one of the three climate zones.

The propagation of the long-wave radiation, in particular the up- and down-welling radiation emitted by the atmosphere itself, as well as changes of this radiation with temperature are derived from radiation transfer calculations [5–7] for each zone.

The *sw* spectral absorptivity, reflecting the solar absorption, is calculated over a spectral range from *0.1–8* μm, and the *lw* spectral absorptivity, characterizing the absorption of the terrestrial and atmospheric radiation, is computed from *3–100* μm. Both these spectra show significant saturation with increasing concentration of water vapour and CO_2 as well as strong mutual interference of these spectra. We explicate, how both effects essentially attenuate the response of the climate system on a changing CO_2 concentration.

The *sw* and *lw* absorptivities are integrated in our climate model to simulate the Earth's surface temperature and the lower tropospheric temperature as a function of the CO_2 concentration. The temperature increase at doubled CO_2 concentration then directly gives the CO_2 climate sensitivity and the respective air sensitivity.

Different scenarios, under clear sky conditions and regular cloud cover, are extensively investigated, including all relevant feedback processes and also the influence of a changing solar activity. These investigations show the dominant impact of a varying cloud cover on global warming, caused by a thermally induced and/or solar induced cloud feedback. In particular, they indicate, that due to this strong cloud feedback the observed warming over the last century can only satisfactorily be explained, attributing a significant fraction to the increased solar activity over this period.

Our simulations predict a climate sensitivity $C_S = 0.6\,^{\circ}C$ and a solar sensitivity $S_S = 0.5\,^{\circ}C$ (*0.1 %* change of the solar constant), whereas the *IPCC* specifies in its actual assessment report [1] the equilibrium climate sensitivity to be likely in the range *1.5* $^{\circ}C$ to *4.5* $^{\circ}C$ (*66-100 %* probability with high confidence) and extremely unlikely less than *1* $^{\circ}C$ (*0-5 %* with high confidence).

2. SPECTROSCOPIC CALCULATIONS

The influence of *GH*-gases on *EASy* is almost exclusively determined by the absorption and emission of these gases in the atmosphere. Therefore, the respective absorption and emission spectra represent the key parameters in any climate model. For the most important *GH*-gases water vapour, carbon dioxide, methane and ozone the *sw* and *lw* absorption is derived from line-by-line calculations based on the HITRAN08-database [4]. Other infrared active gases like N_2O, SF_6 or the halogen-hydrocarbons (halocarbons) with significantly lower concentrations in the atmosphere have no noticeable influence on the further investigations.

Because of the different temperatures and the water content in the atmosphere three climate zones are distinguished: the tropics with an average temperature of *26* $^{\circ}C$, the mid-latitudes with *8* $^{\circ}C$ and the high-latitudes with *-7* $^{\circ}C$.

In this section we briefly explain the underlying principles of our spectral calculations and present the results for the *sw* and *lw* absorptivities, in particular the mutual interference of water vapour and carbon

dioxide with their respective influence on the total absorption.

2.1 Fundamentals

2.1.1 Integral Absorptivity

The spectral intensity of well collimated radiation, transmitting a gas sample, is given by Lambert-Beer's law [5, 6]:

$$I_\lambda(r) = I_\lambda(0) \cdot e^{-\kappa(\lambda,r)} \tag{1}$$

where $I_\lambda(0)$ is the initial spectral intensity on the wavelength λ and $\kappa(\lambda,r)$ the optical depth. In the simplest case $\kappa(\lambda,r)$ is just the product of the absorption coefficient $\alpha(\lambda)$ of the gas and the path length r. Under atmospheric conditions, however, $\alpha(\lambda)$ is varying over the propagation length due to pressure and temperature changes with altitude (z-direction, perpendicular to the surface). Then $\kappa(\lambda,r)$ has to be expressed as an integral of $\alpha(\lambda,r)$ over the path length L. In addition, $\alpha(\lambda,r)$ generally reflects the absorption at λ, caused by different molecular transitions and different gases in the atmosphere. Therefore, $\kappa(\lambda,r)$ assumes the more general form:

$$\kappa(\lambda,L) = \int_0^L \alpha(\lambda,z(r))dr = \int_0^L \sum_k \bar{\alpha}^i_{nm}(\lambda, p^i_p(z(r)), p_t(z(r)), T(z(r)))dr \tag{2}$$

where $\bar{\alpha}^i_{nm}$ represents the effective absorption coefficient, expressing the difference between induced absorption and induced emission processes on an optical or infrared transition between a lower molecular state n and an upper state m [7, 8]. The superscript i distinguishes between the different gas components in the atmosphere. $p^i_p(z(r))$ is the partial pressure of the *i-th* gas, $p_t(z(r))$ the total pressure, $T(z(r))$ the temperature at altitude z and L the path length in the atmosphere. Summation over k expresses the sum over the different transitions and gases.

The integral in (2) is solved numerically by segmenting the atmosphere into up to 228 layers, then calculating the optical depth of each individual layer under the actual conditions at that altitude, and finally summing up over all layers.

The spectral absorptivity also follows from Lambert-Beer's law as:

$$a_\lambda(L) = 1 - t_\lambda(L) = 1 - \frac{I_\lambda(L)}{I_\lambda(0)} = 1 - e^{-\kappa(\lambda,L)} \tag{3}$$

which describes the relative absorption on the wavelength λ or frequency $\nu = c/\lambda$. t_λ is the respective spectral transmissivity and c the speed of light. Then, with (3) the total or integral absorptivity can be defined as:

$$\boldsymbol{a}(L) = \frac{\int_0^\infty I_\lambda(0) \cdot a_\lambda(L)\, d\lambda}{\int_0^\infty I_\lambda(0)\, d\lambda} \times 100 \ [\%] \tag{4}$$

This quantity is quite appropriate to express any radiation losses and by this the absorbed power in the atmosphere over the path length L. Once, calculated for a gas mixture and the respective *sw* or *lw* spectral

distribution I_λ, the absorptivity can quite universally be used to simulate the influence of the gas mixture on the radiation and energy balance of *EASy*. Therefore, the absortivities $\boldsymbol{a}_{SW}$ for the *sw* solar radiation and $\boldsymbol{a}_{LW}$ for the *lw* terrestrial radiation are the key parameters to determine the influence of an increasing CO_2 concentration on global warming.

2.1.2 Atmospheric Pressure and Temperature Changes

The interaction of radiation with gases is considered up to an altitude of *86 km*. For the pressure and temperature variations over this altitude we orientate at the *US Standard Atmosphere* model [9], but introduce some smaller modifications for the individual climate zones *Z*. The standard model uses a global mean ground temperature of *15 ˚C*, and a lapse rate of *6.5 ˚C/km* over the troposphere up to the tropopause, yielding a temperature of *216.65 K* in *11 km* altitude. However, the ground temperatures $T^{Zone}(0)$ of the three zones approximately change over *33 ˚C* (tropics: *26 ˚C = 299.15 K;* mid-latitudes: *8 ˚C = 281.15 K*; high-latitudes: *-7 ˚C = 266.15 K*), whereas at the tropopause the temperatures almost have assimilated to each other (see also subsection 5.4). Therefore, we use a slightly different temperature variation over the troposphere for each of the three climate zones:

$$T^{Zone}(z) = T^{Zone}(0) - \frac{T^{Zone}(0) - 216.65\,K}{11,000\,m}\,z \tag{5}$$

with the respective lapse rates:

$$l_r^{Zone} = -\frac{\Delta T}{\Delta z} = \frac{T^{Zone}(0) - 216.65\,K}{11,000\,m} \tag{6}$$

Due to the different temperature variations and lapse rates also different pressure variations over the troposphere have to be distinguished for the three zones:

$$p^{Zone}(z) = p(z_0)\left(1 - \frac{l_r^{Zone}(z - z_0)}{T(z_0)}\right)^{\frac{M\cdot g}{R\cdot l_r^{Zone}}} \tag{7}$$

with *M = 0.02896 kg/mol* as the molar mass of the atmosphere, *g = 9.81 m/s*^{2} as gravitational acceleration, *R = 8.314 J/K/mol* as universal gas constant and z_0 as reference altitude.

Over the tropopause, the stratosphere and mesosphere again the standard atmosphere model is applied.

2.1.3 Concentration of Greenhouse Gases

Carbon dioxide and methane are well mixed gases in the atmosphere, which are found in almost constant concentrations over the surface and the altitude. Therefore, their number densities, which are important for the absorption strength on a molecular transition, vary proportional with pressure and reciprocal with temperature. Within this paper we use a reference concentration for CO_2 of *380 ppm* and for CH_4 of *1.8 ppm*.

Ozone is distributed over the whole stratosphere and tropopause with a maximum concentration of *7 ppm* around an altitude of *38 km* and extending in downward direction almost down to the troposphere, in upward direction up to the mesosphere.

More complicated but also much more important for the energy and radiation budget in the atmosphere is the water vapour content. It is almost exclusively found in the troposphere up to an altitude of *11 km,* and due to the Clausius-Clapeyron-equation its concentration strongly depends on the temperature, which on the one hand side changes with altitude above ground and on the other hand significantly varies with latitude.

From *GPS*-measurements [10], by which the integral water content in the three climate zones can be determined, together with the temperature and pressure dependence we can calculate the water vapour concentration as a function of altitude (for details see [11]). The mean concentration is in good agreement with the *Average Global Atmosphere*, but almost 2*x* larger than the data derived from the *US Standard Atmosphere* [9], which is only valid for mid-latitudes. The respective graphs for the saturated and unsaturated partial pressures are shown in **Figure 1**. These vapour variations as a function of altitude form the basis for the further spectroscopic calculations.

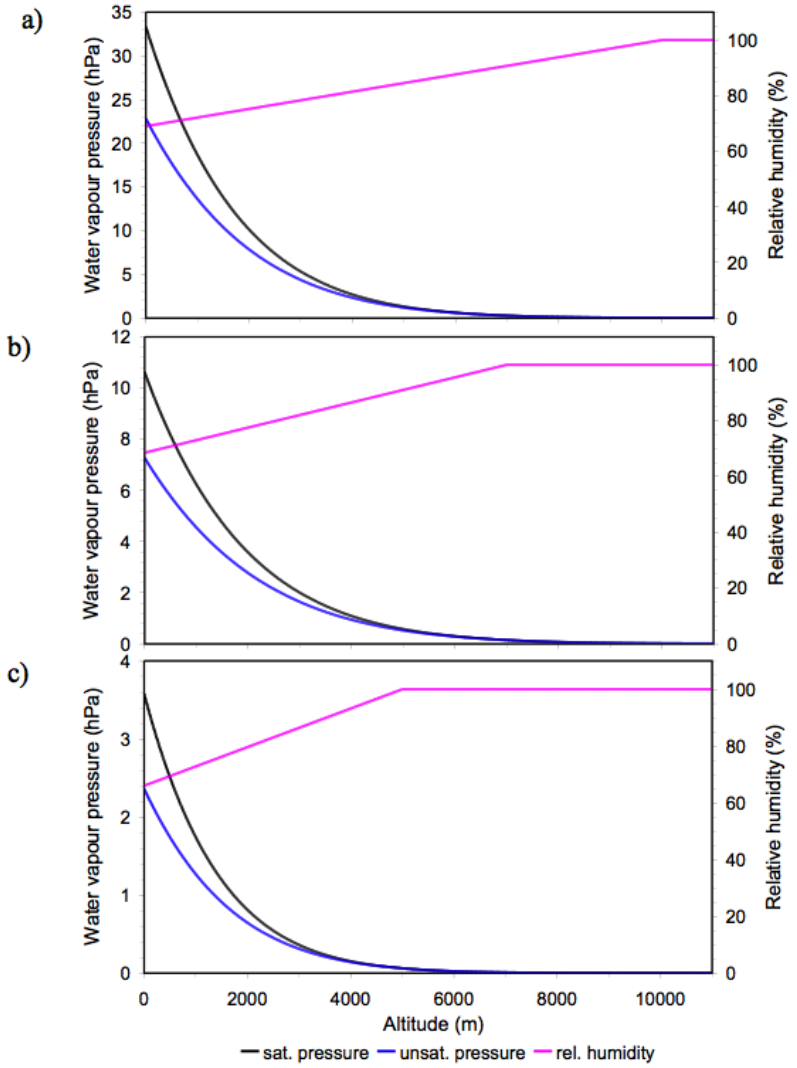

Figure 1. a) Water vapour concentration in the tropics at *26* ^{o}C, b) mid-latitudes at *8* ^{o}C and c) high-latitudes at *-7* ^{o}C as a function of altitude.

2.2 Short-Wave Absorption in the Atmosphere

2.2.1 Path Length in the Atmosphere

Sun light entering the Earth's atmosphere can be considered as a well collimated beam, but due to the spherical shape of the Earth the angle of incidence on an individual gas layer varies with latitude and longitude over 90˚ and by this also the path length, over which absorption within the layer takes place.

In order to restrict the calculations to a finite number of angles and propagation lengths, the earth is considered as a truncated icosahedron (also known as Bucky ball) consisting of 12 pentagonal and 20 hexagonal surface elements (see **Figure 2**).

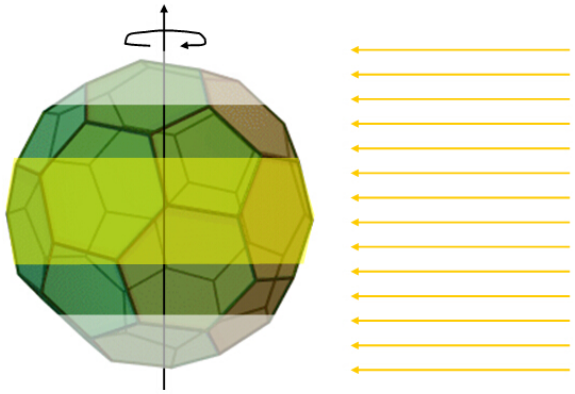

Figure 2. The globe as Bucky ball.

When turning the Bucky ball to a position that a pentagonal area is oriented perpendicular to the incident sun light, further pentagonal and hexagonal areas with specific orientation angles to the sun can be distinguished and respective fractions of them assigned to the three climate zones.

So, as listed in **Table 1**, four different areas contribute to the tropics, three to the mid-latitudes and two to the high-latitudes. Therefore, altogether nine separate calculations, differing in their path lengths and their conditions in the three climate zones, are necessary to determine the *sw* absorptivities.

While the last column in **Table 1** represents the sum of the individual areas for one zone (the total sum gives half the globe surface), for the power irradiating one specific climate zone, the respective projection areas perpendicular to the incident radiation have to be considered.

Table 1. Assigned icosahedron surfaces to the climate zones.

angle of incidence	90˚ - P	52.9˚ - H	25.5˚ - P	11.6˚ - H	area (10^{12} m^2)
tropics	1.0	3.5	2.0	1.5	127.8
mid-latitudes	–	1.5	2.5	2.5	103.5
high-latitudes	–	–	0.5	1	24.4
path in atmosphere (km)	86	108.2	206	535.1	Σ255.8

2.2.2 Absorption Spectrum

Our calculations of the solar absorption in the atmosphere cover a spectral range of *0.1–8 μm* and are based on the HITRAN08-database [4]. Within this spectral interval 60,994 water lines, 262,104 methane lines, and 234,210 carbon dioxide lines are found. Exact calculations with these more than 500,000 lines only contribute to an increased absorption of *0.2%* compared to computations with only the main isotopologues and with spectral line intensities larger than $10^{-24}\ cm^{-1}/(molecules{\cdot}cm^{-2})$. Since this small "offset" is of no concern for further investigations of the CO_2 climate sensitivity, most of the calculations were performed with the reduced number of lines. Within the specified spectral interval this gives for CO_2 4,421 lines, for CH_4 46,208 lines, and for H_2O 9,565 lines.

Since the HITRAN08-database does not include ultraviolet transitions of ozone, we suppose for this gas a continuous absorption between 0.1 and *0.35 μm* with *8 %*. This absorption does not interfere with other contributions of water vapour, CO_2 or CH_4 and is considered separately in the climate model.

The actual spectral calculations, retrieving all the necessary parameters of a molecular transition from the HITRAN08-database and further computing the absorption strength as well as the lineshape for each spectral line as a function of the partial pressures, the total pressure and the temperature over the propagation length, is done by the program platform *MolExplorer* [12].

Figure 3 gives an overview over the transmission and absorption spectrum from *0 - 4 μm*, in this case for the tropics and for perpendicular incidence of the radiation. The spectral solar intensity I_λ can well be approximated by a Planckian blackbody radiator of *5778 K* in good agreement with the observed solar spectrum. It is represented as dotted line in the upper plot and forms the envelope of the transmitted spectrum. The sharp dips and broader white regions indicate the strong absorption at these wavelengths, whereas the lower plot directly represents the respective spectral absorptivity.

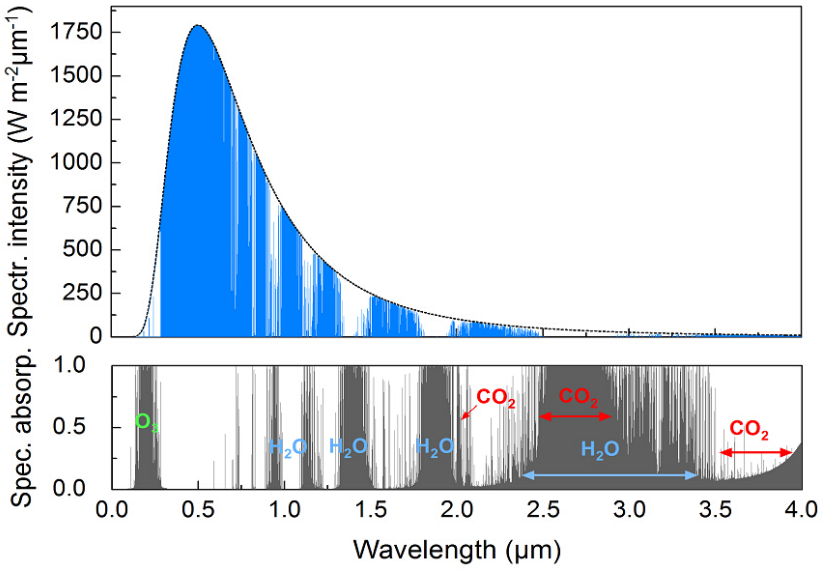

Figure 3. Absorption of sun light in the tropics by H_2O, CO_2, O_3 and CH_4. Above: transmission-, below: absorption-spectrum.

This figure already shows the dominant influence of water vapour over wider spectral regions which alone already contributes to an integral absorptivity of *13.1 %*, while CO_2 only causes *2.24 %* and CH_4

0.22 %. However, with water vapour, that portion which can be attributed to CO_2 and CH_4 (together *2.45%* at standard conditions) reduces to about one quarter of the previous values. The reason is that their absorption bands are strongly overlapping with those of water vapour, so that only *0.52 %*, *i.e.* less than *4 %* of the total absorption, can be allocated to carbon dioxide.

We have calculated the *sw* absorptivities for the three climate zones and also for different CO_2 concentrations from *0-770 ppm*, as listed in **Table 2**. The data of each climate zone and each concentration already represent a weighted average over the projection areas, which contribute to a zone (see **Table 1**). All spectra and by this the respective absorptivities were calculated with a spectral resolution of *1 GHz* or even better.

Table 2. *sw* absorptivities as a function of the CO_2 concentration.

CO_2 (ppm)	*sw* absorptivities a_{sw}(%)			
	tropics	mid-latitudes	high- latitudes	global
0	14.628	12.674	12.267	13.613
35	14.842	12.949	12.658	13.868
70	14.912	13.045	12.800	13.956
140	15.012	13.175	12.974	14.075
210	15.086	13.266	13.092	14.160
280	15.146	13.340	13.182	14.228
350	15.196	13.400	13.255	14.285
380	15.217	13.425	13.284	14.308
420	15.242	13.455	13.319	14.336
490	15.281	13.501	13.373	14.379
560	15.317	13.542	13.420	14.418
630	15.349	13.580	13.461	14.454
700	15.378	13.614	13.498	14.485
770	15.406	13.645	13.533	14.515

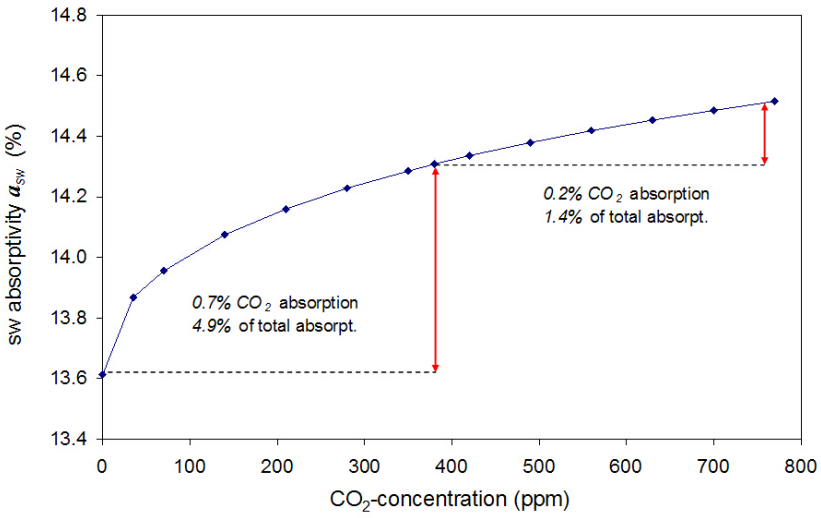

Figure 4. Global *sw* absorptivity as a function of the CO_2 concentration caused by water vapour, CO_2 and CH_4.

The last column in **Table 2** shows the global mean values as the weighted average over the three climate zones. This global *sw* absorptivity is plotted in **Figure 4** as a function of the CO_2 concentration and is used in this form for the further climate simulations. It is obvious, that with increasing concentration the absorption already shows stronger saturation, which in this case means, that within some spectral

regions the atmosphere already becomes completely opaque and only weaker absorption bands or lines can further contribute to an attenuation. So, from zero to *380 ppm* CO_2 the absorption increases by *0.7 %*, whereas a further doubling of CO_2 only contributes to less than *0.2 %*.

2.3 Long-Wave Absorption in the Atmosphere

2.3.1 Spectral Range and Number of Lines

The Earth's surface and the atmosphere, both with temperatures roughly between *-20* and *30* $^\circ C$, represent Planckian radiators, which release part of their collected energy in form of *lw* radiation, but also strongly absorb radiation over the infrared wavelength range. In this subsection we focus on the question, how much of the emitted terrestrial radiation can be absorbed by the atmosphere.

For our spectral calculations we consider a range from *3-100* μm, in which the HITRAN08-database has stored 18,539 water vapour lines, 178,206 methane lines, 167,755 carbon dioxide lines, and 284,647 ozone lines. Again restricting the calculations on the main isotopologues and transitions with spectral intensities larger than 10^{-24} $cm^{-1}/(molecules{\cdot}cm^{-2})$, for water vapour 2,962 lines, for CH_4 17,776 lines, for CO_2 4,454 lines, and for O_3 75,382 lines are left. So, altogether almost 96,000 lines are included in the further investigations. The spectral resolution is again better than *1 GHz*, and the vertical resolution over the atmosphere with up to 228 sub-layers varies from *100 m* over the troposphere up to *1.6 km* in the upper mesosphere.

2.3.2 Propagation of Terrestrial Radiation

Different to the well collimated solar radiation transmitting the atmosphere, terrestrial radiation is emitted by each surface element of the Earth into a solid angle of 2π and is spreading out over the whole hemisphere. In order to determine the absorption of radiation, which is propagating under different directions and covering different distances before exiting an atmospheric layer of thickness *dz*, it is necessary first to consider the interaction of an individual ray with the gas before integrating over all directions.

Supposing the Earth's surface as a Planckian radiator with Lambertian emission, then such an individual beam may be characterized by the spectral radiance $I_{\lambda,\Omega}{\cdot}cos\ \beta{\cdot}\ d\Omega$ emitted under an angle β to the surface normal and into the solid angle interval $d\Omega$ with [6, 7]

$$I_{\lambda,\Omega}\cos\beta\ d\Omega = \frac{2hc^2n^3}{\lambda^5}\frac{1}{e^{\frac{hc}{kT_E\lambda}}-1}\cos\beta\ d\Omega \tag{8}$$

where h is Planck's constant, c the vacuum speed of light, n the refractive index, k the Boltzmann constant and T_E the Earth's surface temperature. This ray covers a distance $dz\,/\,cos\ \beta$ before leaving the layer and, therefore, suffers from absorption losses $\alpha(\lambda)\ I_{\lambda,\Omega}{\cdot}cos\ \beta\,/\,cos\ \beta{\cdot}\ d\Omega\ {\cdot}dz$. Then, integration over Ω gives (see also Ref.[7], (54)):

$$\frac{\int dI_{\lambda,\Omega}\cos\beta\,d\Omega}{dz} = -\sum_k \bar{\alpha}^i_{nm}(\lambda,z)\int_0^{2\pi} I_{\lambda,\Omega}\frac{\cos\beta}{\cos\beta}\,d\Omega = -2\alpha(\lambda,z)\cdot\pi\cdot I_{\lambda,\Omega} \tag{9}$$

where $\alpha(\lambda,z)$ may represent the sum over the effective absorption coefficients of the involved transitions and gases at wavelength λ (see (2)). Since the integral $\int I_{\lambda,\Omega} \cdot cos\ \beta\ d\Omega = \pi \cdot I_{\lambda,\Omega}$ in (9) just defines the spectral intensity I_λ (or spectral flux density) representing the mean expansion of the emitted radiation perpendicular to the surface in z-direction, (9) can be written as

$$\frac{dI_\lambda(z)}{dz} = -2\alpha(\lambda,z) \cdot I_\lambda(z) \tag{10}$$

This differential equation for the spectral intensity shows that the effective absorption coefficient is twice that of the spectral radiance, or in other words the average propagation length of the radiation to pass the layer, is twice the layer thickness. This means, we also can assume radiation, which is absorbed at the regular absorption coefficient $\alpha(\lambda,z)$, but in average is propagating under an angle of 60° to the surface normal ($1/cos\ 60^\circ = 2$).

In reality, the Earth will deviate from a Lambertian radiator and due to Mie scattering or inhomogeneities in the atmosphere the individual rays do not obey geometric optics. Therefore, altogether it seems reasonable to apply a slightly smaller effective absorption coefficient of $(1/cos\ \beta) \cdot \alpha(\lambda,z)$ in (10) with an average propagation angle of $\beta = 52^\circ$. This description is in close agreement with the two-stream approximation (see Ref. 6, $p.232$) and corresponds to a diffusivity factor of $1/cos\ \beta$. Integration of (10) over z and applying (4) then gives the lw absorptivity $\boldsymbol{a}_{LW}$.

2.3.3 Absorption Spectrum

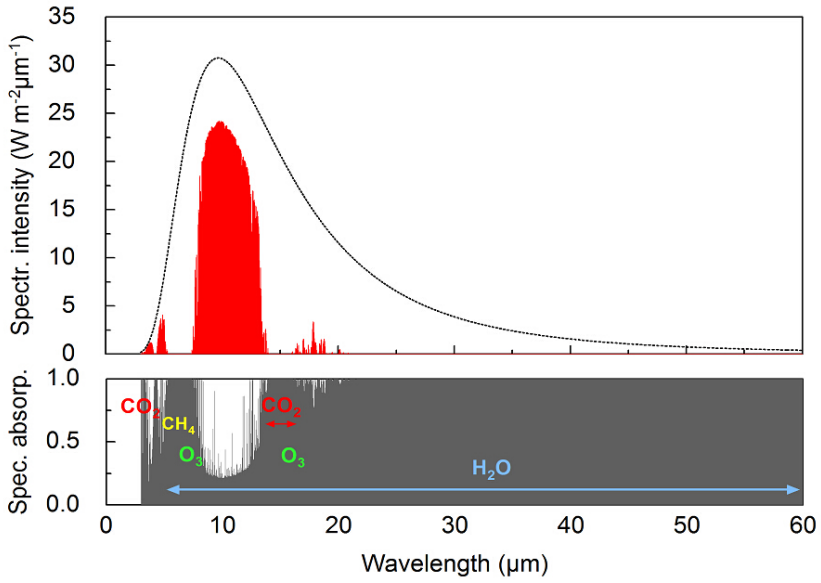

Figure 5. Transmission and absorption spectrum of the terrestrial radiation in the atmosphere.

Figure 5 shows the transmission and absorption spectrum of the terrestrial radiation from $3\text{-}60\ \mu m$ for the tropics with a ground temperature of $26\ ^\circ C$ and a water vapour concentration of $2.29\ \%$. The spectral intensity I_λ for a Planckian blackbody radiator of $26\ ^\circ C$ is plotted as dotted line. The total flux as the integral over the spectral intensity in this case is $I_E = 454 W/m^2$, from which $85.7\ \%$ are absorbed by the

GH-gases. Over wider spectral regions the atmosphere is almost completely opaque, only around *10* μm less than *15 %* of the terrestrial radiation can directly be released to space. Again by far the largest amount of the absorption results from water vapour, which already contributes to *80.1 %*, whereas CO_2 alone delivers *22.9 %*, CH_4 *2.0 %* and O_3 *3.3 %*. However, due to the overlap with the water vapour spectrum in the presence of the other gases CO_2 only causes an additional increase of the *lw* absorptivity of *3.5 %*.

The calculated *lw* absorptivities for the three climate zones as a function of the CO_2 concentration are listed in **Table 3**. The values in the second last column again represent the weighted averages over the three climate zones. These averages, however, slightly deviate by about *1%* from calculations performed under conditions with a unique temperature of *15.5* $^{\circ}C$ and a unique water vapour concentration of *14,615 ppm*. These values for the temperature and vapour concentration were also determined as weighted averages over the climate zones. The absorptivities calculated with these global mean parameters are listed in the last column of **Table 3** and are plotted as a function of the CO_2 concentration in **Figure 6**.

Table 3. *lw* absorptivities as a function of the CO_2 concentration.

CO_2 (ppm)	*lw* absorptivities α_{LW} (%)				
	tropics	mid-latitudes	high- latitudes	average 3 zones	global mean
0	81.90	69.44	58.98	74.68	77.02
35	83.80	74.48	67.04	78.43	80.08
70	84.18	75.35	68.32	79.10	80.62
140	84.65	76.31	69.80	79.86	81.29
210	84.99	77.00	70.77	80.40	81.76
280	85.28	77.51	71.52	80.83	82.14
350	85.53	77.95	72.14	81.19	82.45
380	85.65	78.12	72.38	81.34	82.58
420	85.76	78.33	72.68	81.51	82.74
490	85.97	78.67	73.16	81.80	83.00
560	86.16	78.98	73.61	82.06	83.24
630	86.35	79.29	74.02	82.32	83.46
700	86.52	79.58	74.41	82.56	83.68
770	86.69	79.85	74.78	82.79	83.88

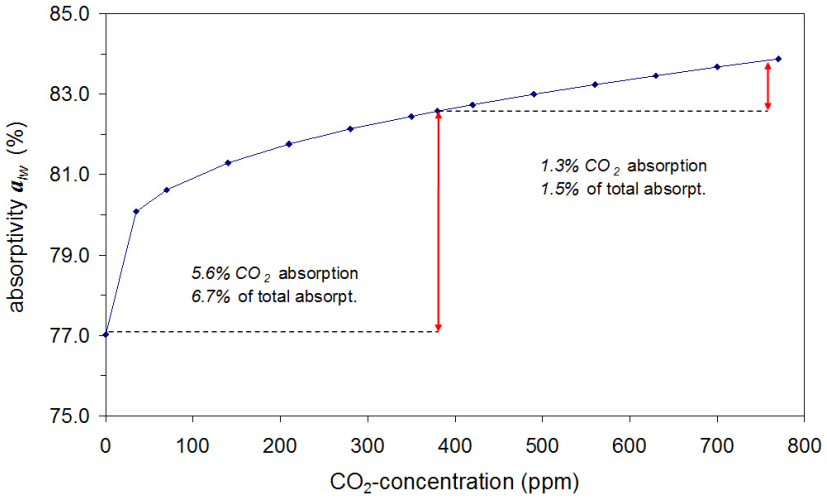

Figure 6. Global *lw* absorptivity as a function of the CO_2 concentration caused by water vapour, CO_2, CH_4 and O_3.

Since in this paper we particularly focus on the global influence of CO_2, characterized by the global

climate sensitivity, it seems appropriate to use these data for our further simulations. In any way, it is found that for the climate sensitivity it makes no bigger difference, which data set is used.

Similar to the *sw* absorptivities also the *lw* radiation suffers from stronger saturation effects with increasing concentration. So, from zero to *380 ppm* the absorption increases by *5.6 %* whereas a further doubling of the CO_2 concentration only contributes to about *1.3 %*.

3. RADIATION TRANSFER IN THE ATMOSPHERE

In the previous section we were focusing on the absorption of solar and terrestrial radiation in the atmosphere, both increasing the mechanical, kinetic and inner energy of the gaseous cover. But in thermal equilibrium the atmosphere has to release the same amount of energy to space - and also some fraction back to the surface - as it accepts by absorbed radiation and heat transfer. This mostly appears via radiation processes in upward and downward direction, since in the same way, as *GH* gases are strong absorbers, they are also strong emitters of infrared radiation.

Therefore, a more extensive analysis of the energy and radiation balance of the atmosphere not only accounts for the net absorbed power from the incident radiation, as considered in (1)-(4) and (10), but it also includes any radiation originating from the atmosphere itself as well as any re-radiation due to an external excitation. This is the subject of this section.

3.1 Radiation Transfer Equation for the Spectral Radiance

When considering radiation, which transmits the atmosphere and on its way suffers from absorption losses, this radiation simultaneously is superimposed by thermal radiation originating from spontaneous emission of infrared active molecules in the atmosphere. Since this emission almost covers the same wavelength range as the terrestrial radiation, it can significantly reduce the effective absorption losses of a beam, it can modify the spectral distribution or can be the origin of new up- and down-welling radiation in the atmosphere.

The spectral power density on the wavelength λ due to spontaneous emission of the different gases i on the transitions $m \rightarrow n$ into the full solid angle of 4π is:

$$\frac{du_\lambda}{dt} = \sum_k h\nu_{mn} A^i_{mn} N^i_m g^i(\nu, \nu_{mn}) = \sum_k \frac{hc}{\lambda_{mn}} A^i_{mn} N^i_m g^i(\lambda, \lambda_{mn}) \tag{11}$$

and represents a spectral generation rate of photons of energy $h\nu_{mn}$ per volume. u_λ is the spectral energy density, ν_{mn} the resonance transition frequency, λ_{mn} the respective resonance wavelength, A_{mn} the Einstein coefficient for spontaneous emission, N_m the number density of an excited molecular state m and $g(\lambda,\lambda_{mn})$ the lineshape function of a molecular transition [7].

Therefore, over small propagation distances dr in the atmosphere both contributions, the radiation losses and the thermal emission, can be summed up, and for the spectral radiance $I_{\lambda,\Omega}$ we can write:

$$\frac{dI_{\lambda,\Omega}(r)}{dr} = -\sum_k \bar{\alpha}^i_{nm}(\lambda) \cdot I_{\lambda,\Omega}(r) + \frac{1}{4\pi} \sum_k \frac{hc}{\lambda_{mn}} A^i_{mn} N^i_m(r)\, g^i(\lambda, \lambda_{mn}) \tag{12}$$

While the first term is known from Lambert-Beer's law, representing the absorption and emission processes induced by the incident radiation, the second term describes the spontaneous emission on the different molecular transitions contributing to the spectral radiance at wavelength λ. Summation over k again means the sum over individual transitions within one molecule and over the different gases indicated by the superscript i.

Photons emerging from a volume element spread out into the neighbouring areas, but also arrive from the neighbourhood. In a homogeneous medium both fluxes just compensate each other. Nevertheless, in a dense atmosphere as found within the troposphere, photons have an average lifetime, before they are annihilated due to an absorption in the gas. Of course, this is the case for the incident radiation, as represented by the first term in (12), but in the same way this happens to the thermal background radiation. With an average photon lifetime

$$\tau_{ph}(\lambda) = l_{ph}(\lambda)\frac{n}{c} = \frac{n}{c}\frac{1}{\sum \bar{\alpha}^i_{nm}(\lambda)} \tag{13}$$

where $l_{ph} = 1/\sum \bar{\alpha}^i_{nm}$ is the mean free path of a photon in the gas, before it is absorbed on the wavelength λ, at thermal equilibrium we can write for the spectral energy density:

$$u_\lambda = \frac{h \cdot n}{\sum\limits_k \bar{\alpha}^i_{nm}(\lambda)} \cdot \sum_k \frac{A^i_{mn}}{\lambda_{mn}} N^i_m g^i(\lambda, \lambda_{mn}) \tag{14}$$

As already outlined previously ([7], subsection 2.5), u_λ just represents the spectral energy density of a Planckian radiator at λ and is given by

$$u_\lambda = \frac{8\pi n^4 hc}{\lambda^5}\frac{1}{e^{\frac{hc}{kT_A\lambda}} - 1} = \frac{4\pi n}{c} B_{\lambda,\Omega}(T_A) \tag{15}$$

with $B_{\lambda,\Omega}(T_A)$ as the Kirchhoff-Planck function, which is identical with (8) but now describes the spectral radiance of the atmosphere at temperature T_A.

With (14) and (15) then the second term in (12) can be expressed by the respective absorption coefficients on a transition, times the Kirchhoff-Planck function:

$$\frac{dI_{\lambda,\Omega}(r)}{dr} = -\sum_k \bar{\alpha}^i_{nm}(\lambda, r) \cdot I_{\lambda,\Omega}(r) + \sum_k \bar{\alpha}^i_{nm}(\lambda, r) \cdot B_{\lambda,\Omega}(T_A(r)) \tag{16}$$

This equation is known as the Schwarzschild equation [5–7, 13], which describes the propagation of radiation in an absorbing gas and in the presence of thermal background radiation of this gas. Generally this equation is derived from pure thermodynamic considerations and is valid under conditions, when the collision rate C_{mn} of superelastic collisions (transitions from $m \rightarrow n$ due to de-exciting, non-radiating collisions) is much larger than the spontaneous emission rate A_{mn}. Typically this is the case within the whole troposphere up to the stratosphere.

For our calculations from the surface up to the mesopause and vice versa we use a generalized form of the radiation transfer equation (see Ref. 7):

$$\frac{dI_{\lambda,\Omega}(r)}{dr} = \sum_k \bar{\alpha}^i_{nm}(\lambda, r)\left(-\chi(r) \cdot I_{\lambda,\Omega}(r) + B_{\lambda,\Omega}(T_A(r))\right) \tag{17}$$

which can also be derived from (12) and covers both limiting cases of thin and dense atmospheres. In particular, it allows a continuous transition from low to high densities, controlled by a collision dependent parameter $\chi(r)$ [7]:

$$\chi(r) = 1 - \frac{1/4}{1 + C_{mn}(r)/A_{mn}} \tag{18}$$

which can adopt values from $3/4 \leq \chi \leq 1$ for $0 \leq C_{mn}/A_{mn} \leq \infty$.

3.2 Radiation Transfer Equation for the Spectral Intensity

Since for the further considerations the radiation emitted into the full hemisphere is of interest, (17) has to be integrated over the solid angle $\Omega = 2\pi$. As already discussed in subsection 2.3, a beam, propagating under an angle β to the layer normal (z-direction), only contributes an amount $I_{\lambda,\Omega}\ cos\beta \cdot d\Omega$ to the spectral intensity due to Lambert's law. The same is assumed to be true for the thermal radiation emitted by a gas layer under this angle.

On the other hand the path length through a layer of depth dz is increasing with $dr = dz/cos\beta$, so that the β-dependence for both terms $I_{\lambda,\Omega}$ and $B_{\lambda,\Omega}$ disappears.

Therefore, analogous to (9) integration of (17) over Ω and using the identities $I_\lambda = \pi \cdot I_{\lambda,\Omega}$ as well as $B_\lambda = \pi \cdot B_{\lambda,\Omega}$, gives for the spectral intensity in z-direction:

$$\frac{dI_\lambda(z)}{dz} = 2\sum_k \bar{\alpha}^i_{nm}(\lambda, z)\left(-\chi(z) I_\lambda(z) + B_\lambda(T_A(z))\right) \tag{19}$$

Since the density of the gases, the total pressure and the temperature are changing with altitude, (19) has to be solved stepwise for thin layers of thickness Δz, over which the absorption coefficients $\bar{\alpha}^i_{nm}$, the parameter χ and the spectral intensities I_λ and B_λ can be assumed to be constant. With the running index j for different layers then (19) can be calculated stepwise by (see Ref. 7, subsection 4.5):

$$I^j_\lambda(\Delta z) = I^{j-1}_\lambda e^{-2\chi^j \Sigma \bar{\alpha}^{i,j}_{nm}(\lambda)\Delta z} + \frac{1}{\chi^j} B^j_\lambda(T^j_A) \cdot (1 - e^{-2\chi^j \Sigma \bar{\alpha}^{i,j}_{nm}(\lambda)\Delta z}) \tag{20}$$

The intensity in the *j-th* layer is computed from the previous intensity I^{j-1}_λ of the *(j-1)-th* layer with the values $\bar{\alpha}^{i,j}_{nm}(\lambda)$ and $B^j_\lambda(T^j_A)$ of the *j-th* layer. In this way the propagation over the full atmosphere is calculated stepwise.

The first term in (20) describes the transmission of the incident spectral intensity in a lossy medium over the layer thickness, whereas the second term represents the self-absorption of the thermal background radiation in forward direction and is identical with the spontaneous emission of the layer into one hemisphere.

Similar to (10) also for the radiation transfer calculations we apply slightly smaller effective absorption coefficients by replacing $2\bar{\alpha}^{i,j}_{nm}(\lambda)$ in the exponents of (20) by $\bar{\alpha}^{i,j}_{nm}(\lambda)/\cos\beta$ and assuming an average propagation direction of $\beta = 52^\circ$.

3.3 Radiation Transfer Calculations

An example of the calculated radiation transfer from the earth's surface to *TOA* (*86 km* altitude) for the tropics is shown in **Figure 7**.a. The temperature and pressure dependence over the atmosphere is assumed to be the same as used in section 2. The surface is considered as a blackbody radiator at 26˚C with a spectral intensity shown as the red dotted graph and with a total emitted intensity $I_E = 454\ W/m^2$. On its way through the atmosphere the radiation experiences significant absorption, except over the spectral window around $10\ \mu m$. Nevertheless, the intensity released to space is less attenuated than expected from the strongly saturated absorption bands of CO_2 and water vapour (see **Figure 5**). Spectral regions of strong absorption just also emit very intensively, only at reduced temperatures at higher altitudes and therefore at reduced intensity.

The total outgoing intensity I^{up}_{total} at *TOA* as the integral over the spectrum of **Figure 7**.a can be explained to consist of the non-absorbed terrestrial intensity $(I_E - I_{abs})$ plus the upwelling intensity of the atmosphere I^{up}_A with:

$$I^{up}_{total} = I_E - I_{abs} + I^{up}_A \tag{21}$$

Figure 7.b shows the up-welling spectral intensity, only caused by the emission of the atmosphere itself, and integrated over λ this gives I^{up}_A . The difference of both graphs a) and b) determine the absorption of terrestrial radiation in the atmosphere, whereas the difference of the integrated curves and normalized to the initial terrestrial intensity I_E yields the respective absorptivity as listed in section 2.

So, from this point of view application of the radiation-transfer-model would give no new insight. Sometimes it even leads to some misinterpretation, that the CO_2 absorption on the $15\ \mu m$ band would not be saturated. However, for the understanding and interpretation of satellite and ground based spectra [7, 14–21] these calculations are indispensable and their excellent agreement with the measurements confirm the correct theoretical basis for the radiation transfer in the atmosphere. Related to the radiation and energy balance of *EASy* they are particularly important to evaluate, which fraction of the total thermal background radiation is rejected to space and what is emitted in downward direction to be absorbed by the surface.

Figure 7.c represents a plot, which was calculated under identical conditions as before, but showing the down-welling radiation, which has piled up from zero at *TOA* to significant strength at the surface, only originating from spontaneous emission of the *GH*-gases in downward direction. Over wider spectral regions the intensity is almost identical to a blackbody radiator, only within the spectral window around $10\ \mu m$ a deeper hole in the spectral distribution, similar to **Figure 7**.b, can be observed.

In the tropics the intensity in downward direction is *80%* of a blackbody radiator at $26\,^{\circ}C$ and corresponds to *63 %* of the total atmospheric emission, whereas the outgoing fraction only contributes to *37%*. The reason for this asymmetric emission of the atmosphere is the lapse rate and to some degree also the density profile over the atmosphere, which both are responsible, that the lower and warmer layers are radiating more intensively than the higher, colder layers. This asymmetric radiation of the atmosphere can be expressed by an asymmetry factor:

$$f_A = \frac{\int_0^{\infty} I^{down}_{\lambda,A}\, d\lambda}{\int_0^{\infty} I^{up}_{\lambda,A}\, d\lambda + \int_0^{\infty} I^{down}_{\lambda,A}\, d\lambda} \times 100\,[\%] \tag{22}$$

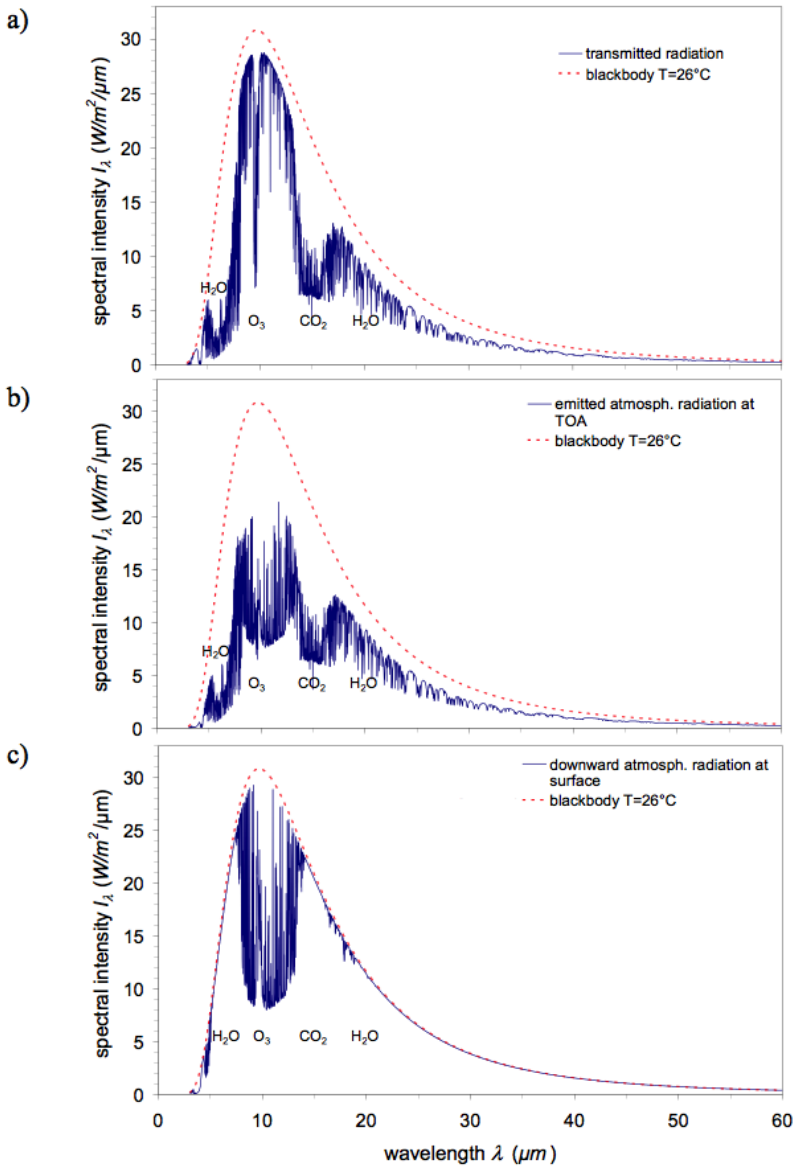

Figure 7. a) Total outgoing radiation at the top of the atmosphere (*TOA*) in the tropics, b) up-welling and c) down-welling spectral intensity only of the atmosphere, calculated by the radiation transfer model.

when $I^{down}_{\lambda,A}$ and $I^{up}_{\lambda,A}$ are the down- and up-welling spectral intensities emitted by the atmosphere.

Because of the different ground temperature, the varying lapse rate, and humidity also these intensities are changing with the climate zones and, therefore, f_A is not a fixed parameter but varies over these zones (see **Table 4**). **Figure 8** shows f_A as a function of the ground temperature T_E (red triangles). This graph can well be represented by a straight line with a slope $df_A/dT_E = 0.145\ \%/^\circ C$, which defines the temperature dependence of f_A and has some further consequences on the lapse rate feedback, as this will be discussed in section 5.

The additionally plotted values for f_A, calculated for deviations of $\pm 5\ ^\circ C$ from the mean temperature of a climate zone, indicate the slightly smaller temperature influence, when the humidity is held fixed within a climate zone.

Table 4. Calculated intensities, *lw* absorptivities, and asymmetry factor f_A in the three climate zones at standard conditions.

zone T (˚C)	intensity (W/m^2)						f_A(%)	$\boldsymbol{a}_{LW}$(%)
	I_E	I_{total}^{up}	I_A^{up}	I_A^{down}	I_A^{total}	I_{abs}		
high-lat.: -7	284.50	221.02	142.94	194.09	337.03	206.26	57.59	72.38
mid-lat.: 8	354.27	249.85	172.97	259.63	432.60	277.01	60.02	78.12
tropics: 26	454.09	282.16	218.10	364.58	582.68	389.11	62.57	85.65

Table 4 also presents the *lw* absorptivies in the three climate zones, as derived from the radiation transfer calculations, and **Figure 8** shows this as a function of the temperature (blue squares). Under conditions as defined in section 2, $\boldsymbol{a}_{LW}$ can also well be represented by a straight line with a slope $d\boldsymbol{a}_{LW}/dT_E = 0.38$ %/˚C. This relation directly connects the *lw* absorptivities via the water vapour concentration with the temperature and thus, determines the water vapour feedback. At fixed humidity, the absorptivity would evidently decrease with rising temperature, as this can be seen within the individual climate zones.

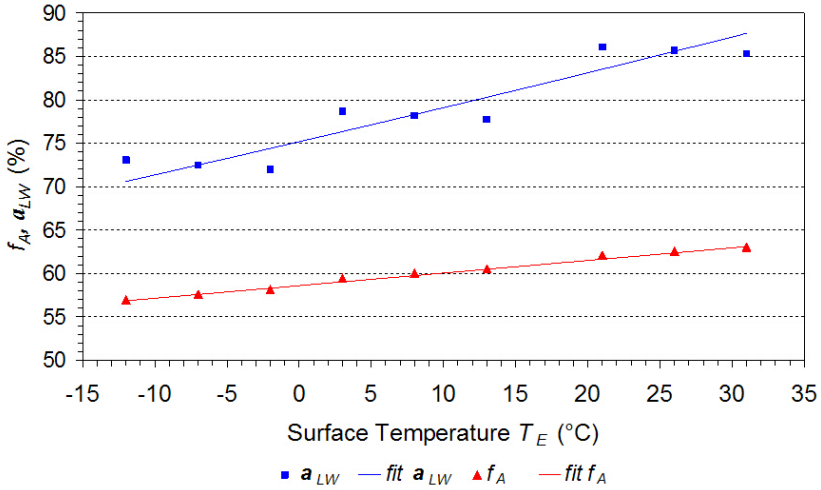

Figure 8. Asymmetry factor f_A and *lw* absorptivity $\boldsymbol{a}_{LW}$ as a function of the ground temperature T_E.

4. ADVANCED TWO-LAYER CLIMATE MODEL

The driving force of *EASy* is the absorbed solar energy in the atmosphere and at the Earth's surface. This energy is converted into heat, internal energy, potential and kinetic energy or radiation, and generally it is quite inhomogeneously distributed over the globe, causing stronger temporal and local redistribution and exchange processes in lateral and vertical directions. Nevertheless, in average none of these processes contribute to the globally integrated transfers between the surface, the atmosphere and the space. Over time scales long compared with those for the redistribution of the energy, *EASy* can be assumed to be in thermal equilibrium. This will be the basis for the further considerations.

The presented calculations of the *sw* and *lw* absorptivities in the atmosphere, as discussed in sections 2 and 3, directly determine the energy balance and by this the temperatures, adjusting between the surface and the atmosphere.

In this section we consider a two-layer-climate model, consisting of the surface as one layer and the

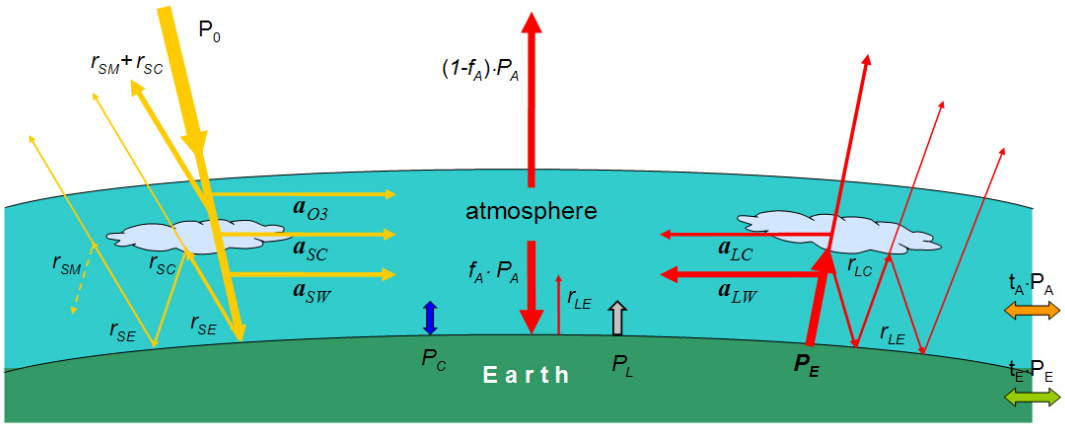

Figure 9. Two-layer climate model of the Earth's surface and atmosphere.

atmosphere as a second, wider layer (see **Figure 9**), both acting as absorbers and Planck radiators. In this aspect it is similar to the Dines or Liou models [22–24], however, with a lot more features, *e.g.*, the *sw* and *lw* absorptivities, caused by the varying gas concentrations or temperature, and also including cloud effects for the *sw*- and *lw*-radiation, sensible and latent heat transfer as well as all relevant feedback effects like water vapour, lapse rate, albedo, cloud cover, convection and evaporation.

In equilibrium the surface and atmosphere each donate as much power as they accept from the sun, the neighbouring layer or a conterminal climate zone.

4.1 Short-Wave Radiation Budget

The solar power irradiating one of these climate zones (tropics, mid-latitudes or high-latitudes) is:

$$P_0 = E_S \cdot A^Z_{pro} \tag{23}$$

with A^Z_{pro} as the projection area perpendicular to the incident light and E_S as the solar constant. Then, the power absorbed by O_3 over the stratosphere and tropopause and mostly released as heat in the atmosphere, may be

1. to atmos:

$$\boldsymbol{a}_{O3} \cdot P_0 \tag{24}$$

where $\boldsymbol{a}_{O3}$ is the integral absorptivity of the O_3 molecules.

On its further way through the atmosphere the non-absorbed portion $(1\text{-}\boldsymbol{a}_{O3}) \cdot P_o$ will partially be backscattered to space, for which two cases have to be distinguished. Under clear sky conditions primarily Rayleigh and Mie scattering by molecules and micro-sized particles in the atmosphere will be observed. This process may be characterized by a scattering coefficient r_{SM} for sun light or *sw* radiation (although physically not correct, often designated as reflection). With cloud overcast additional scattering occurs with an increased scattering coefficient r_{SA}, which may be expressed as sum of the molecular and an additional cloud scattering contribution r_{SC} with $r_{SA} = r_{SM} + r_{SC}$, and which is weighted with the cloud cover C_C. Then the total sun light scattered back to space is:

1. to space:

$$((1-C_C)r_{SM}+C_C r_{SA})\cdot(1-\boldsymbol{a}_{O3})P_0=(r_{SM}+C_C\cdot r_{SC})\cdot(1-\boldsymbol{a}_{O3})\cdot P_0 \tag{25}$$

Radiation propagating through clouds not only suffers from stronger scattering losses but also from an additional absorption over the cloud path. With a cloud absorptivity $\boldsymbol{a}_{SC}$ the spare power which is released as heat energy in the atmosphere becomes

2. to atmos:

$$\boldsymbol{a}_{SC}C_C(1-r_{SA})\cdot(1-\boldsymbol{a}_{O3})P_0 \tag{26}$$

The down-welling radiation also consists of two parts, one representing the clear sky conditions with weight (1 - C_C), the other the cloud covered portion with weight C_C. On its further path to the surface additional absorption losses due to water vapour, CO_2 and CH_4 show up, which for simplicity are assumed to occur primarily in the lower troposphere. With an absorptivity $\boldsymbol{a}_{SW}$ we find for the power, transferred to the atmosphere:

3. to atmos:

$$\boldsymbol{a}_{SW}\left[(1-C_C)(1-r_{SM})+C_C(1-r_{SA})(1-\boldsymbol{a}_{SC})\right]\cdot(1-\boldsymbol{a}_{O3})P_0 \tag{27}$$

As a first contribution, which can be coupled to the surface layer, it is left:

1. to Earth:

$$(1-r_{SE})(1-\boldsymbol{a}_{SW})\left[(1-C_C)(1-r_{SM})+C_C(1-r_{SA})(1-\boldsymbol{a}_{SC})\right]\cdot(1-\boldsymbol{a}_{O3})P_0 \tag{28}$$

where r_{SE} is the reflectivity of the Earth's surface for *sw* radiation.

The reflected radiation from the surface not only disappears to space but can again be scatted at the atmosphere as molecular and cloud scattering, and can also further be absorbed in the clouds. The reflected power at the surface is

$$r_{SE}\cdot(1-\boldsymbol{a}_{SW})\left[(1-C_C)(1-r_{SM})+C_C(1-r_{SA})(1-\boldsymbol{a}_{SC})\right]\cdot(1-\boldsymbol{a}_{O3})P_0=r_{SE}\cdot PS \tag{29}$$

with the abbreviation *PS* for Power at the Surface. An additional absorption of this outgoing radiation by water vapour and CO_2 can well be neglected due to saturation effects and bleaching of the radiation on the stronger absorption bands. But radiation passing again the clouds delivers a second contribution to the atmosphere:

4. to atmos:

$$C_C(1-r_{SA})\,\boldsymbol{a}_{SC}\cdot r_{SE}PS \tag{30}$$

and the amount passing to space is:

2. to space:

$$((1-C_C)(1-r_{SM})+C_C(1-r_{SA})(1-\boldsymbol{a}_{SC}))\cdot r_{SE}PS \tag{31}$$

That part, again scattered down and coupled into the surface, is

2. to Earth:

$$(1-r_{SE})((1-C_C)r_{SM}+C_C r_{SA})\,r_{SE}\cdot PS \tag{32}$$

After a second reflection at the surface we find the contributions:

5. to atmos:

$$C_C(1-r_{SA})\,\boldsymbol{a}_{SC}\cdot r_{SE}\,((1-C_C)r_{SM}+C_C r_{SA})\cdot r_{SE}PS \tag{33}$$

3. to space:

$$((1-C_C)(1-r_{SM})+C_C(1-r_{SA})\,(1-\boldsymbol{a}_{SC}))\cdot r_{SE}\,((1-C_C)r_{SM}+C_C r_{SA})\cdot r_{SE}PS \tag{34}$$

3. to Earth:

$$(1-r_{SE})\cdot r_{SE}^2((1-C_C)r_{SM}+C_C r_{SA})^2\cdot PS \tag{35}$$

A third reflection at the surface gives:

6. to atmos:

$$C_C(1-r_{SA})\,\boldsymbol{a}_{SC}\cdot r_{SE}^2((1-C_C)r_{SM}+C_C r_{SA})^2\cdot r_{SE}PS \tag{36}$$

4. to space:

$$((1-C_C)(1-r_{SM})+C_C(1-r_{SA})\,(1-\boldsymbol{a}_{SC}))\cdot r_{SE}^2((1-C_C)r_{SM}+C_C r_{SA})^2\cdot r_{SE}PS \tag{37}$$

4. to Earth:

$$(1-r_{SE})\cdot r_{SE}^3((1-C_C)r_{SM}+C_C r_{SA})^3\cdot PS \tag{38}$$

It is easy to be seen that additional reflections contribute to three power series which under typical conditions rapidly converge and can be represented by their sum formulas. So, listing up the individual contributions for the atmosphere, the Earth and space this gives:

atmos:

$$P_{S\to A}=\left\{\begin{array}{r}\boldsymbol{a}_{O3}+\boldsymbol{a}_{SC}C_C(1-r_{SA})(1-\boldsymbol{a}_{O3})+\left[\boldsymbol{a}_{SW}+\frac{r_{SE}\boldsymbol{a}_{SC}C_C(1-r_{SA})(1-\boldsymbol{a}_{SW})}{1-r_{SE}((1-C_C)r_{SM}+C_C r_{SA})}\right]\times\\ [(1-C_C)(1-r_{SM})+C_C(1-r_{SA})(1-\boldsymbol{a}_{SC})]\cdot(1-\boldsymbol{a}_{O3})\end{array}\right\}P_0 \tag{39}$$

Earth:

$$P_{S\to E}=(1-r_{SE})(1-\boldsymbol{a}_{SW})\cdot\frac{[(1-C_C)(1-r_{SM})+C_C(1-r_{SA})(1-\boldsymbol{a}_{SC})]}{1-r_{SE}\,((1-C_C)r_{SM}+C_C r_{SA})}\cdot(1-\boldsymbol{a}_{O3})\cdot P_0 \tag{40}$$

space:

$$P_{S\to Sp}=\left\{r_{SM}+C_C r_{SC}+r_{SE}\cdot\frac{[(1-C_C)(1-r_{SM})+C_C(1-r_{SA})(1-\boldsymbol{a}_{SC})]^2}{1-r_{SE}\,((1-C_C)r_{SM}+C_C r_{SA})}\cdot(1-\boldsymbol{a}_{SW})\right\}\times(1-\boldsymbol{a}_{O3})\cdot P_0 \tag{41}$$

4.2 Long-Wave Radiation Budget

Most of the energy transfer between the two layers occurs through *lw* radiation, since both the surface and the atmosphere act as absorbers and Planckian radiators in the mid-infrared (*IR*). The power P_E emitted by the surface, is absorbed over wider spectral regions by water vapour, CO_2 and CH_4 within the lower troposphere, and an additional fraction of *1.5 %* by O_3 in the stratosphere. With an absorptivity $\boldsymbol{a}_{LW}$ for the *lw* radiation the amount

1. to atmos:

$$\boldsymbol{a}_{LW} \cdot P_E \tag{42}$$

is absorbed and released in the atmosphere, whereas the non-absorbed fraction can directly escape to deep space (Rayleigh scattering in the *IR* is negligible) or is partially backscattered by clouds to the surface. At a cloud cover C_C and a cloud scattering coefficient r_{LC} for *lw* radiation then the fraction

1. to Earth:

$$(1-r_{LE})C_C r_{LC}(1-\boldsymbol{a}_{LW}) \cdot P_E \tag{43}$$

is coupled back to the surface, where r_{LE} represents the reflectivity of *lw* radiation at the surface.

That portion which is not backscattered but penetrates into clouds, again splits into a stronger absorptive contribution and a smaller residuum escaping to space. Denoting the cloud absorptivity for *lw* radiation as $\boldsymbol{a}_{LC}$, the power absorbed by the clouds and further transferred to the atmosphere is:

2. to atmos:

$$C_C(1-r_{LC})\boldsymbol{a}_{LC}(1-\boldsymbol{a}_{LW}) \cdot P_E \tag{44}$$

With (44) we assume that the absorbed radiation is totally released as internal energy or heat in the atmosphere due to dominating heat conduction and convection processes. A slightly modified picture would be that the absorbed power is re-radiated by the clouds, and because of the continuous broad Planck spectrum only part of this radiation is reabsorbed by the *GH*-gases in the atmosphere, whereas from the non-resonant fraction one half goes to space, the other half is rejected down to the surface. However, a detailed comparison shows that both pictures almost give identical results in the energy balance, and since the reality might be somewhere between, here we restrict our further discussion on the first assumption.

The power disappearing to space consists of that portion propagating through clear sky areas, and a rest having transmitted the clouds:

1. to space:

$$((1-C_C)+C_C(1-r_{LC})(1-\boldsymbol{a}_{LC})) \cdot (1-\boldsymbol{a}_{LW}) \cdot P_E \tag{45}$$

That radiation, backscattered (*1st* time) from clouds and then reflected at the ground, is again split into the three parts:

3. to atmos:

$$C_C^2 r_{LE} r_{LC}(1-r_{LC})\boldsymbol{a}_{LC}(1-\boldsymbol{a}_{LW}) \cdot P_E \tag{46}$$

2. to Earth:

$$C_C^2 r_{LC}^2 r_{LE}(1-r_{LE})(1-\boldsymbol{a}_{LW}) \cdot P_E \tag{47}$$

2. to space:

$$C_C r_{LC} r_{LE} \cdot ((1-C_C)+C_C(1-r_{LC})(1-\boldsymbol{a}_{LC})) \cdot (1-\boldsymbol{a}_{LW}) \cdot P_E \tag{48}$$

A next round trip delivers the contributions:

4. to atmos:

$$C_C^3 r_{LE}^2 r_{LC}^2 (1-r_{LC}) \boldsymbol{a}_{LC} (1-\boldsymbol{a}_{LW}) \cdot P_E \tag{49}$$

3. to Earth:

$$C_C^3 r_{LC}^3 r_{LE}^2 (1-r_{LE})(1-\boldsymbol{a}_{LW}) \cdot P_E \tag{50}$$

3. to space:

$$C_C^2 r_{LC}^2 r_{LE}^2 \cdot ((1-C_C) + C_C (1-r_{LC})(1-\boldsymbol{a}_{LC})) \cdot (1-\boldsymbol{a}_{LW}) \cdot P_E \tag{51}$$

Including further reflections and scattering events leads again to respective power series for the two layers and the space. Summing up all these contributions and taking into account the initial radiation loss P_E from the Earth's surface we find:

atmos:

$$P_{E\to A} = \left\{ \boldsymbol{a}_{LW} + \frac{C_C}{1-C_C r_{LE} r_{LC}} (1-r_{LC}) \boldsymbol{a}_{LC} (1-\boldsymbol{a}_{LW}) \right\} \cdot P_E \tag{52}$$

Earth:

$$P_{E\to E} = -\left\{ 1 - \frac{C_C r_{LC}}{1-C_C r_{LE} r_{LC}} (1-r_{LE})(1-\boldsymbol{a}_{LW}) \right\} \cdot P_E \tag{53}$$

space:

$$P_{E\to Sp} = \frac{1}{1-C_C r_{LE} r_{LC}} [(1-C_C) + C_C (1-r_{LC})(1-\boldsymbol{a}_{LC})] \cdot (1-\boldsymbol{a}_{LW}) \cdot P_E \tag{54}$$

The atmosphere also represents a Planckian radiator, which emits the power P_A. Due to the temperature distribution over altitude a smaller fraction (1 - f_A) $\approx$ *39 %* of this *lw* radiation escapes to space (see (22)), the other part $f_A \approx 61\%$ is directed downward. At the surface some smaller fraction of the down-welling radiation is reflected back and remains in the atmosphere, whereas the main part is absorbed by the surface. This supplements the *lw* radiation balance for the two layers and the space, for which we find:

atmos:

$$P_{A\to A} = -((1-f_A) + f_A - r_{LE} f_A) \cdot P_A = -(1 - r_{LE} f_A) \cdot P_A \tag{55}$$

Earth:

$$P_{A\to E} = (1-r_{LE}) f_A \cdot P_A \tag{56}$$

space:

$$P_{A\to Sp} = (1-f_A) \cdot P_A \tag{57}$$

4.3 Sensible and Latent Heat

Most of the energy transfer between the surface and atmosphere occurs by *lw* absorption and emission processes. However, additional energy can be transferred through sensible and latent heat. While sensible heat represents the energy transfer through thermal conduction and convection from the warmer to the colder layer, latent heat describes the energy transfer resulting from phase transitions of evaporating water

or sublimating ice at the surface and subsequent release of the vaporization energy in the atmosphere, when the water vapour condenses and falls back as precipitation.

Therefore, the total energy balance between the surface and atmosphere has to be supplemented by the heat transfer between both layers.

The driving force for thermal conduction and convection is the temperature difference at the boundary layer between surface and atmosphere. In addition, advection in form of a horizontal energy transfer along the boundary through wind and water currents takes place. This transfer is only indirectly dependent on the temperature difference, therefore, it is close-by to assume a power transfer through sensible heat, represented by a temperature independent portion P_{C0} and a temperature dependent part in the form:

$$P_C = P_{C0} + h_C A^Z (T_E - T_{AC}) \tag{58}$$

with h_C as the heat transfer coefficient, A^Z as the surface area of a climate zone, T_E as the Earth's surface temperature and T_{AC} as the air temperature at the convection zone.

An energy transfer from the surface to the atmosphere through latent heat is directly affected by the temperature T_E of the surface, since with increasing temperature more water is evaporating and more precipitation expected. Generally latent heat just represents the difference in enthalpy for the transformation between two phases of consideration, and according to Kirchhoff's equation (see, *e.g.* [6], $p.123$), changes in latent heat are directly proportional to temperature changes with a proportionality factor, given by the difference of the specific heats in the two phases. To allow some smaller deviations from this general response over a wider temperature interval, and on the other hand to express only changes in latent heat around a point of reference - this is of particular interest for our considerations here - we assume a similar relationship for latent heat as applied for sensible heat:

$$P_L = P_{L0} + l_H A^Z (T_E - T_0) \tag{59}$$

with P_{L0} as a fixed contribution defining the point of reference, T_0 as the freezing temperature, and l_H as the respective heat coefficient.

For an energy budget, which is restricted to a specific climate zone, an additional exchange between these zones through atmospheric and oceanic currents has to be included. The power transfers P_{TA} in the atmosphere and P_{TE} along the Earth's surface to or from an adjacent zone are governed by energy differences and heat fluxes between the zones. Since any changes in the energy budget also retroact on the transfer between two zones and such changes are directly reflected by the radiated powers, the transfer between adjacent zones may be expressed in units of P_A and P_E. Then, with an increasing or decreasing balance in one zone in first order also the flux to or from a neighbouring region is changing as:

$$P_{TA} = t_A \cdot P_A \ \ resp. \ \ P_{TE} = t_E \cdot P_E \tag{60}$$

with t_A and t_E as transfer factors for the atmospheric and terrestrial heat transfer. They are negative, when the net flux from a considered zone goes out, and they are positive, when power is sucked up.

4.4 Total Radiation and Energy Budget

At thermal equilibrium the absorbed solar radiation must be balanced by the net emission of *lw* radiation of *EASy* to space. This is conservation of energy and the demand of the first law of thermodynamics.

A balance for each layer, and complementarily for space, gives a coupled equation system describing the mutual interdependence of the power fluxes between the layers and space.

For the atmosphere we sum up the in- and outgoing fluxes listed in equations (39), (52), (55) and (58)-(60), for the Earth those listed in (40), (53), (56), (60) and (58)-(59) with opposite sign, and for the space the radiation terms of (41), (54) and (57), which just must balance the incident solar power:

Atmosphere:

$$P_{S\to A} + P_{A\to A} + P_{E\to A} + P_C + P_L + P_{TA} = 0 \tag{61}$$

Earth:

$$P_{S\to E} + P_{A\to E} + P_{E\to E} - P_C - P_L + P_{TE} = 0 \tag{62}$$

Space:

$$P_{S\to Sp} + P_{A\to Sp} + P_{E\to Sp} = P_0 \tag{63}$$

To identify the mutual coupling of P_E and P_A, in more elaborate form these equations can be written as:

Atmosphere:

$$P_{S\to A} - \alpha P_A + A P_E + P_C + P_L = 0 \tag{64}$$

Earth:

$$P_{S\to E} + \beta P_A - B P_E - P_C - P_L = 0 \tag{65}$$

Space:

$$P_{S\to Sp} + \gamma P_A + C P_E = P_0 \tag{66}$$

with the abbreviations:

$$\alpha = 1 - r_{LE} f_A - t_A \quad \beta = (1 - r_{LE}) f_A \quad \gamma = 1 - f_A \tag{67}$$

$$A = \boldsymbol{a}_{LW} + \frac{C_C}{1 - C_C r_{LE} r_{LC}} (1 - r_{LC}) \boldsymbol{a}_{LC} (1 - \boldsymbol{a}_{LW}) \tag{68}$$

$$B = 1 - t_E - \frac{C_C r_{LC}}{1 - C_C r_{LE} r_{LC}} (1 - r_{LE}) (1 - \boldsymbol{a}_{LW}) \tag{69}$$

$$C = \frac{1}{1 - C_C r_{LE} r_{LC}} [(1 - C_C) + C_C (1 - r_{LC})(1 - \boldsymbol{a}_{LC})] \cdot (1 - \boldsymbol{a}_{LW}) \tag{70}$$

The upper equation system is over-determined, since one relation, *e.g.*, the balance for space is already implicitly a consequence of the other two relations and only expresses right away the conservation of radiation energy at the *TOA*. Thus, for a further elucidation of an adjusting equilibrium between the layers only two of these equations are of relevance. Here we further rely on the upper two equations (64) and (65).

In the special case of known sensible and latent heat, the remaining balance equations can easily be solved yielding:

$$P_E = \frac{\alpha P_{S\to E} + \beta P_{S\to A} - (\alpha - \beta)(P_C + P_L)}{\alpha B - \beta A} \tag{71}$$

$$P_A = \frac{1}{\alpha}\left\{P_{S\to A} + P_C + P_L + A \cdot \frac{\alpha P_{S\to E} + \beta P_{S\to A} - (\alpha - \beta)(P_C + P_L)}{\alpha B - \beta A}\right\}. \tag{72}$$

In general, however, P_C and P_L are no fixed quantities, but at least to some degree are directly influenced by the energy balance between the layers and therewith by the respective temperatures T_E and T_A (see (58)-(59)).

When the Earth and the atmosphere are considered as black- or grey-body radiators, emitting the radiation power P_E at an average surface temperature T_E and the power P_A at a mean atmospheric temperature T_A, the Stefan-Boltzmann law [5, 6] provides a well-known relationship between the radiated power and the temperature. For the Earth's surface as a Planckian radiator this gives:

$$P_E = \varepsilon_E \cdot \sigma \cdot A^Z \cdot T_E^4 \tag{73}$$

with the emissivity ε_E of the surface and the Stefan-Boltzmann constant $\sigma = 5.67 \cdot 10^{-8} W/m^2/K^4$.

To characterize also the atmosphere by an average temperature according to Stefan-Boltzmann, we have to have in mind, that due to the asymmetric radiation of the atmosphere, a fraction f_A is emitted downward and (1 - f_A) upward. As a consequence we have to distinguish between two mean temperatures $T_{A,l}$ and $T_{A,u}$ characterizing the lower and the upper troposphere, and defined by the relations:

$$f_A \cdot P_A = \varepsilon_A \cdot \sigma \cdot A^Z \cdot T_{A,l}^4 \tag{74}$$

$$(1 - f_A) \cdot P_A = \varepsilon_A \cdot \sigma \cdot A^Z \cdot T_{A,u}^4 \tag{75}$$

Whereas (75) is not further needed for the succeeding discussion, (74) is relevant to embrace any feedback of the convection to the total balance. Since $T_{A,l}$ typically reflects a temperature, equivalent to an air layer temperature in about 800m altitude, but convection is only dominant over about 200m height, the temperature difference $(T_E - T_{AC})$ in (58) is assumed to be just one quarter of the difference $(T_E - T_{A,l})$. For simplicity we write for the lower tropospheric temperature only T_A. So, for the further considerations (58) may be replaced by

$$P_C = P_{C0} + {}^1\!/_4 h_C A^Z (T_E - T_A) \tag{76}$$

The relations (73) and (74) then represent a link between the balance equations (64)-(65) on the one hand side and the sensible and latent heat ((76) and (59)) on the other side. Together all these relations form a nonlinear equation system, in which the radiation and heat fluxes are coupled to each other via the temperatures T_E and T_A.

This equation-system can be solved iteratively. With initial conditions $P_C = P_{C0}$ and $P_L = P_{L0}$, in a first step initial values for P_E and P_A are calculated by means of the balance equations, and with (73)-(74) initial values for the temperatures T_E and T_A are derived. According to (76) and (59) with these temperatures first improved values for P_C and P_L are found, which in a next iteration step are inserted in (64)-(65) to find new powers and temperatures. This procedure is repeated till the calculations show self-consistency.

To evaluate the influence of CO_2 on global warming and by this to determine the CO_2 climate sensitivity, this kind of calculation has to be performed at different CO_2 concentrations, at least at the

actual concentration as a reference and, *e.g.*, the doubled concentration. Due to the changing *sw* and *lw* absorptivities at these different concentrations also the radiation and energy balance will be altered and therewith the temperatures. Since any deviation from the reference temperature causes a chain of additional feedback processes, in a second loop these feedbacks are included and the calculations are consecutively repeated until also with these corrections self-consistency for the temperature values is found.

5. SIMULATIONS WITHOUT SOLAR INFLUENCE

The *sw* and *lw* absorptivities were calculated for global conditions as well as for the three climate zones. Therefore, also individual simulations for each climate zone could easily be performed. However, comparison with radiation and energy budget data for theses zones are quite restricted. So, here we only consider simulations for the global Earth-atmosphere system. Nevertheless the separate spectral calculations are important, to derive from these data the water vapour and lapse rate feedback as outlined in section 3. In this section only simulations of global warming, caused by CO_2 alone will be presented. The additional influence of solar variations will be discussed in section 6.

5.1 Adaptation to Satellite Measurements

For our simulations we use parameter values as listed in **Table 5**. The *sw* and *lw* absorptivities result from the calculations presented in section 2 and are valid for standard atmospheric conditions with a mean water vapour concentration at ground of *1.46 %*, a CO_2 concentration of *380 ppm*, a CH_4 concentration of *1.8 ppm* and a varying O_3 concentration over the stratosphere with a maximum around *38 km* altitude. The average cloud cover with $C_C = 66\%$ was adopted from published data of the *International Satellite Cloud Climatology Project* (*ISCCP*) [25]. The other parameters like cloud and *sw* ozone absorptivities, the scattering coefficients at clouds and the atmosphere as well as the Earth's reflectivities were adapted in such a way that all radiation and heat fluxes almost exactly reproduce the widely accepted radiation and energy budget scheme of Tremberth, Fasullo and Kiehl [20] (hereafter TFK-scheme, see **Figure 10**), which essentially relies on data from satellite measurements within the *ERBE* and *CERES* program [15–19]. So, this adaptation quasi yields a calibration of our model to the observed up- and down-welling fluxes under standard conditions in the atmosphere and for constant heat fluxes between the surface and atmosphere.

A quite important parameter for reproducing the TFK-scheme is the asymmetry factor f_A, which specifies the amount of downward directed *lw* radiation in comparison to the totally emitted power of the atmosphere. Therefore, it directly determines the *lw* fluxes in up- and downward direction, and by this controls the *lw* radiation balance. Its size sensitively depends on the lapse rate and the ground temperature, but also on the water vapour content and the diffusivity factor. From our radiation transfer calculations (see section 3) we find variations from *57.6 - 62.6 %* over the climate zones and an averaged value of f_A = *61.0 %*. We achieve good consistency with the TFK-data for $f_A = 61.8\ \%$, therefore, this value will be used in the further computations.

Comparison of our simulations with the TFK-scheme (see **Table 6**) then shows quite good agreement to each other and by this confirms the basically correct and reliable operation of the presented model.

Table 5. Parameters for adaptation to the TFK-data.

parameter	symbol	unit	value
total solar irradiance - *TSI*	E_s	W/m^2	1365.2
averaged solar flux	$I_{S,av}$	W/m^2	341.3
Earth's surface area	A_E	$10^{12}m^2$	510
projection area	A_{pro}	$10^{12}m^2$	128
Cloud cover	C_C	%	66.0
sw molec. scattering coef.	r_{SM}	%	10.65
sw cloud scattering coef.	r_{SC}	%	22.0
sw Earth reflectivity	r_{SE}	%	17.0
sw absorptivity: ozone	a_{O3}	%	8.0
sw cloud absorptivity	a_{SC}	%	12.39
sw absorptivity: H_2O-CO_2-CH_4	a_{SW}	%	14.51
lw cloud scattering coef.	r_{LC}	%	19.5
lw Earth reflectivity	r_{LE}	%	0.0
lw cloud absorptivity	a_{LC}	%	62.2
lw absorpt.: H_2O-CO_2-CH_4-O_3	a_{LW}	%	82.58
Earth emissivity	$\varepsilon_E = 1 - r_{LE}$	%	100.0
atmosph. emissivity	ε_A	%	87.5
asymmetry factor	f_A	%	61.8
sensible heat flux	P_C/A_E	W/m^2	17.0
latent heat flux	P_L/A_E	W/m^2	80.0

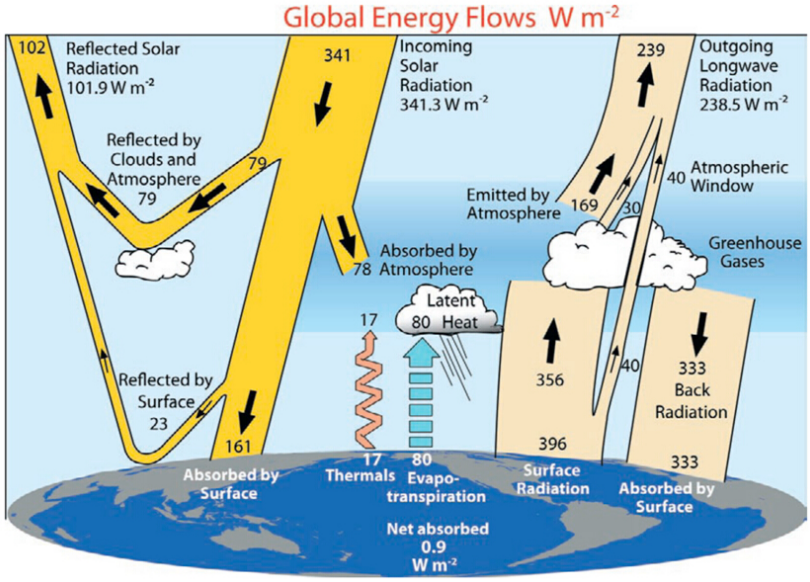

Figure 10. Radiation and Energy Budget of the Earth-atmosphere system (after Tremberth, Fasullo and Kiehl [20], reproduced with permission of the authors).

A smaller systematic deviation, however, results from the fact that the up- and down-welling fluxes in the TFK-scheme are not completely balanced, but contribute to a net surface absorption of $0.9W/m^2$. Therefore, the total outgoing radiation, in our data 239.4 W/m^2, is by this amount larger, and a similar discrepancy with opposite sign appears for the back-radiation with some smaller feedback also on the f_A-factor.

It should also be noticed, that Tremberth *et al.* use a terrestrial radiation flux, which corresponds to a global mean temperature of $16\,^{\circ}C$ instead of the generally applied $15\,^{\circ}C$. This discrepancy can be

Table 6. Calculated radiation fluxes and comparison with the TFK-data.

flux (W/m^2)	this model	TFK-data
sw: incoming solar radiation	341.3	341.3
backscattered from molecules	11.4	
backscattered from clouds	67.6	
together backscattered	79.0	79
reflected at Earth's surface	22.9	23
total reflected solar radiation	101.9	101.9
absorbed by O_3,	27.3	
clouds,	19.1	
water vap, CO_2, CH_4	31.6	
total absorption atmosphere	78.0	78.0
absorption in surface	161.3	161
lw: surface radiation	396.4	396
absorbed by *GH*-gases	322.4	
absorbed by clouds	24.4	
backscattered by clouds	9.5	
absorb. & scat. surface radiation	356.3	356
sensible heat	17.0	17
latent heat	80.0	80
total absorption in atmosph.	521.8	
outgoing radiation fr. atmosph.	199.4	199
outgoing directly from surface	40.0	40
total outgoing radiation	239.4	238.5
backradiation	332.0	333
net emission of surface	64.4	
total outgoing radiation at *TOA*	341.3	340.4

explained by different averaging procedures applied to derive a global mean and from this to calculate the radiated power by the Stefan-Boltzmann law.

Somewhat surprising is, that they assume a reflectivity for *lw* radiation at the surface of $r_{LE} = 0$ and therefore an emissivity $\varepsilon_E = 1 - r_{LE} = 1$, although it is mentioned in their paper that the Earth is no ideal blackbody radiator and in some areas the reflectivity is at least several %. To maintain the otherwise good conformity to the TFK-scheme, in this frame we assume also a zero Earth reflectivity for *lw* radiation and use a ground temperature of $16\,^{\circ}C$.

Since the objective of our further investigations is to evaluate the influence of CO_2 on global warming, we use the specified parameters in **Table 5** as reference marks, which in some sense define a working point for the further considerations, in particular they determine the reference temperature of the Earth's surface at a CO_2 concentration of *380 ppm*. Only deviations from this reference, caused by a changing CO_2 concentration and the different feedback processes, are of further interest, not so much absolute temperature levels.

5.2 Influence of some Model-Parameters on the Balance

In order to assign the influence and importance of the different parameters, it seems worthwhile first to discover the response of the global system to any changes of these parameters. This is a prerequisite for a better understanding and interpretation of the complex heating and cooling effects which partially amplify but also erase each other.

There is no doubt that the *sw* and *lw* absorptivities of the *GH*-gases have a dominant influence on

any balance between the two layers. This will be discussed in more detail in the next subsection. But also the cloudiness, characterized by the key parameter cloud cover C_C as well as the *sw* and *lw* scattering coefficients and absorptivities have a significant affect on this balance, and this even in a somewhat ambiguous way. While a reduced cloud cover generally causes surface heating due to the higher transmissivity of the atmosphere for solar radiation, at the same time this also increases the transparency for the outgoing *lw* radiation from the surface to space and therefore contributes to a stronger cooling. So, to some degree both effects can compensate each other, depending on the actual weather conditions, the day time, or in our simulations depending on the choice of the scattering and absorption parameters.

The rejected solar radiation at the atmosphere and clouds with $79\ W/m^2$ can easily be adjusted by one or both *sw* scattering coefficients, which together determine the total backscattered flux according to (25):

$$((1-C_C)r_{SM}+C_C r_{SA})\cdot(1-\boldsymbol{a}_{O3})P_0=(r_{SM}+C_C\cdot r_{SC})\cdot(1-\boldsymbol{a}_{O3})\cdot P_0 \qquad (25)$$

with $r_{SA}=r_{SM}+r_{SC}$. However, the response of *EASy* to any changes in the cloud cover additionally depends on the weighting of r_{SC} in comparison to r_{SM} , and also on the size of the *lw* cloud scattering r_{LC}.

In our simulations these parameters are adjusted in such a way, that on the one hand side the fluxes agree with the TFK-data, on the other side they reproduce the observations of the global mean temperature change with cloud cover. From the *ISCCP*-data [25] it is found that *1 %* of a reduced cloud cover causes a temperature increase of about *0.06 - 0.07 °C*. This tendency is also confirmed by data of Hartmann [26], well knowing that such observations are superimposed by several other effects influencing the temperature data. With the parameter set in **Table 5** we can well reproduce this temperature response to the cloud cover with a global mean temperature of *19.8 °C* at C_C = *0 %* and *13.0 °C* at *100%* overcast.

The cloud absorptivities and surface reflectivities are not very sensitive parameters with respect to consequences on the climate sensitivity, but their correct choice insures the right adaptation of the total atmospheric and surface absorptions. In this sense they define the reference temperatures at which the two layers are found in equilibrium.

It should be noticed that the *sw* and *lw* cloud and ground absorptions are generally the result of multiple up and down scattering events, at least as long as the reflections at the surface are not zero. Therefore, the listed fluxes and absorptions in **Table 6** cannot simply be derived by multiplying the incident or outgoing radiation with the respective absorptivity or reflectivity, but have to be calculated using some of the relations considered in subsections 4.1 or 4.2, *e.g.*, the *sw* reflection at the surface with $22.9\ W/m^2$ is not only a function of the ground reflectivity with r_{SE} = *17 %* but is additionally influenced by several other parameters (see also (41)):

$$I_R=((1-C_C)\cdot(1-r_{SM})+C_C(1-r_{SA})\cdot(1-\boldsymbol{a}_{SC}))^2\cdot\frac{r_{SE}(1-\boldsymbol{a}_{SW})\cdot(1-\boldsymbol{a}_{O3})}{1-r_{SE}\left(C_C r_{SA}+(1-C_{C)})r_{SM}\right)}\cdot\frac{E_S}{4} \qquad (77)$$

So, an effective reflectivity, related to the incident solar flux at *TOA*, is only *22.9/341.3·100 = 6.7 %*, or with respect to the primary flux (before the first reflection at surface) is *22.9/186.1·100 = 12.3 %*.

While the surface emissivity ε_E has a direct influence on the *lw* radiation budget, but was set to unity to agree with the TFK-scheme, the atmospheric emissivity ε_A in our model is only needed to calculate the mean temperature of the lower troposphere, which affects the temperature dependent part of thermal convection between the layers (see (76)) and insofar also causes a direct feedback on the adjusting balance. Generally the atmospheric emissivity is identical to the total *lw* absorptivity as given by (68) with:

$$\varepsilon_A=A=\boldsymbol{a}_{LW}+\frac{C_C}{1-C_C r_{LE} r_{LC}}(1-r_{LC})\,\boldsymbol{a}_{LC}(1-\boldsymbol{a}_{LW}) \qquad (78)$$

and, therefore, consists of the absorption caused by *GH*-gases as well as of the cloud absorption. Since $\boldsymbol{a}_{LW}$ is varying with the CO_2 concentration, also ε_A becomes a function of this concentration, but owing to the second term in (78) on a slightly varying background. This is in so far of some importance, since an atmospheric temperature, calculated from the balance equations with the emissivity of (78), shows a significantly lower sensitivity to concentration variations than assuming a constant emissivity, as this is generally applied. As a direct consequence the sensible heat flux increases with the CO_2 concentration and causes additional cooling of the surface, thus leading to a negative feedback in the *EASy*-balance.

5.3 Direct Influence of CO_2 on the Surface-Temperature

GH-gases have a twofold influence on the *EASy* energy and radiation budget. While they attenuate the solar radiation and by this the amount which can be absorbed by the surface, they block a great deal of the terrestrial radiation to be directly rejected to space and thus, cumber the energy loss to space. In **Table 2** and **Table 3** are compiled the integral *sw* and *lw* absorptivities of the well-mixed *GH*-gases water vapour, CO_2, CH_4 *and* O_3 . They were derived from line-by-line calculations and determined for different CO_2 concentrations from *0-770 ppm*. To assess the influence of CO_2 on global warming, we use these absorptivities and calculate for each pair of *sw* and *lw* absorptivities at otherwise identical conditions the respective surface and atmospheric temperature. For the case of clear sky ($C_C = 0$) this is shown in **Figure 11**.a. The red graph indicates the Earth's temperature T_E and the blue graph the lower tropospheric temperature T_A. The increase of T_E at doubled CO_2 concentration (from *380 to 760 ppm*) defines the CO_2 climate sensitivity as a measure for the response of *EASy* on a changing CO_2 concentration. In this case, at clear sky conditions and without any feedback effects, we find a climate sensitivity of $C_S = 1.11\,^{\circ}C$ which is in surprisingly good agreement with the *IPCC* value also of $C_S = 1.1\,^{\circ}C$ (without feedback processes, but generally assuming mean cloud cover) and based on the *RF*- concept [2, 3]. Additionally shown is a logarithmic plot (green graph), indicating that due to saturation effects and only far wing absorption at higher CO_2 concentrations the surface temperature can well be approximated by a logarithmic function.

From **Figure 11**.a we also see that the lower atmosphere responds less sensitively to the CO_2 changes. The respective temperature increase of T_A at doubled CO_2, which we may call here as air sensitivity, is only $A_S = 0.45\,^{\circ}C$ and significantly smaller than the climate sensitivity. This lower response is explained by the fact that with increasing CO_2 concentration also the emissivity of the atmosphere is increasing (see (78)) and so compensating to some degree the higher absorption in the atmosphere.

The dominant influence of clouds on the whole energy budget can be seen from **Figure 11**.b. When repeating the same calculation as before, only choosing the mean cloud cover of *66 %*, not only the temperatures are considerably dropping (T_E by $3.8\,^{\circ}C$, T_A by $2.8\,^{\circ}C$), but also the climate and air sensitivities are significantly reducing to $C_S = 0.55\,^{\circ}C$ and $A_S = 0.19\,^{\circ}C$.

While the falling temperatures are a consequence of the dominating shielding effect for solar radiation (in the real climate system particularly caused by the lower clouds), the smaller sensitivities are a direct consequence of the increasing influence of the *lw* cloud absorption and backscattering, by which the importance of the *GH*-gases is more and more repelled. So, at *100 %* cloud cover the air sensitivity would completely disappear and the climate sensitivity be reduced to $0.2\,^{\circ}C$.

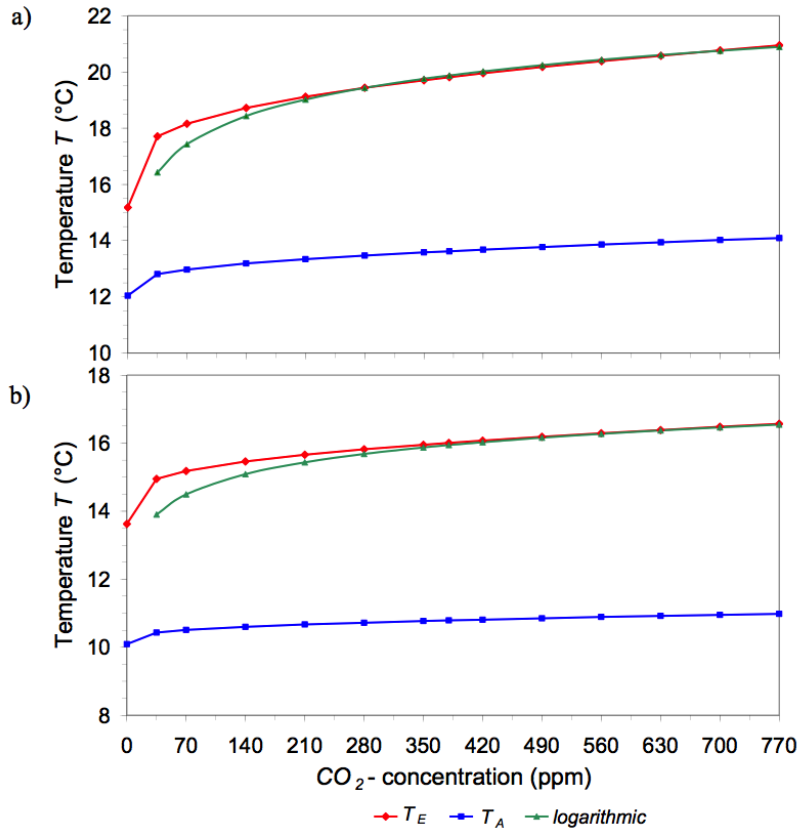

Figure 11. Calculated Earth-temperature T_E (red) and lower tropospheric temperature T_A (blue) as a function of the CO_2 concentration under a) clear sky, b) *66%* cloud cover. Logarithmic approximation - green.

5.4 Feedback Processes

Most of the climate scientists agree, that an increasing absorption with rising CO_2 concentration alone, as discussed in the previous subsection, would only moderately contribute to any global warming. The greater worry, however, is that already smaller perturbations, as caused by the *GH*-effect, may initiate further side effects, which could significantly amplify the primary perturbation and even result in a total destabilization of the quasi equilibrium conditions of *EASy*. These side-effects are known as feedback processes, which on one side can amplify an initial deviation (positive feedback) or on the other side can also attenuate this deviation (negative feedback).

5.4.1 Water-Vapour-Feedback

Due to the Clausius-Clapeyron-equation the water vapour content in air is rapidly increasing with rising temperatures. Therefore, also the water vapour absorption is further increasing and generally contributes to a positive feedback in the total budget. In the literature this feedback is designated as the most serious effect with dramatic amplification values of 1.5 - 3 [27].

Our own investigations, however, show a less dramatic influence of water vapour. One aspect is that,

similar to CO_2, also the water lines are already strongly saturating over wider spectral regions. Therefore, with increasing vapour concentration only the far wings of these lines and weak absorption bands can further contribute to an additional absorption, which roughly logarithmically increases with the vapour concentration.

In this context, obviously some physical misinterpretation of the absorption behaviour of a gas exists, see *e.g.* Ref. 27. So, it is concluded that not the absolute change in the water vapour concentration, but its fractional change would govern the strength as a feedback mechanism; and from this statement it is deduced, that the largest contribution to the feedback occurs in the upper troposphere. However, molecules can only absorb radiation, which is still available on the absorption frequencies. Since the lower atmospheric layers with the strongly pressure broadened spectral lines already filter the outgoing radiation up to the far wings and by this determine the logarithmic absorption behaviour, there is no further radiation left for the narrower lines in the upper troposphere, only from adjacent layers of the atmosphere itself. In addition, the absorption strength on the line centre, and thus the saturation behaviour for the radiation, is almost the same in the upper troposphere as in the lower troposphere, since with reducing pressure and temperature on the one hand the number of molecules decreases, but due to the reducing linewidth the linestrength increases. This is the law of spectral stability.

Another aspect is that always both, the *sw* and *lw* absorptions have to be considered. While the *lw* outgoing radiation is more efficiently blocked and so contributes to positive feedback, the *sw* radiation is also stronger absorbed in the atmosphere, but less of it reaches the surface and therefore supplies a net negative feedback.

Our calculations for the *sw* and *lw* absorptivities in section 2 were performed for three climate zones, which differ in their mean humidity and ground temperature. **Figure 12** shows the absorptivities in these zones as a function of the respective ground temperatures at *380 ppm* CO_2.

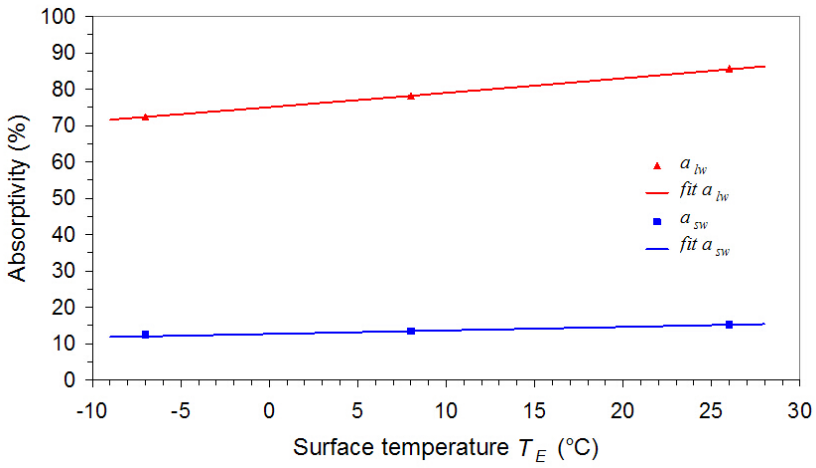

Figure 12. Calculated *sw* absorptivity (blue) and *lw* absorptivity (red) for the three climate zones plotted as a function of the respective zone temperatures.

Since the water content in each climate zone was derived from actual *GPS*-measurements [10] and this water content used to calculate the water vapour concentration at this zone-temperature, the graphs in **Figure 12** directly reflect the temperature dependence of the water vapour concentration on the absorptivities. The linear increase is the result of an exponential growth of the water vapour concentration with temperature due to Clausius-Clapeyron and on the other hand a logarithmic rise of the absorptivity

with the vapour concentration due to saturation effects.

The sw and *lw* absorptivities can well be represented by straight lines with the slopes

$$d\boldsymbol{a}_{SW}/dT_E = 0.097\ \%/^{\circ}C \tag{79}$$

and

$$d\boldsymbol{a}_{LW}/dT_E = 0.38\ \%/^{\circ}C \tag{80}$$

With these parameters the water vapour feedback can be included in the further considerations by an iterative procedure, as already outlined in section 4. In a first step the temperature deviation from the reference temperature T_R, caused by a deviation of CO_2 from the reference concentration (here 380 ppm) is calculated. This T-offset is used to compute with the feedback parameters the corrections in the absorptivities. With the new values again corrected temperatures are determined, which give new absorption corrections. This is repeated, until the temperatures show self-consistency.

The result of such calculation is illustrated in **Figure 13**, representing the temperature increase of T_E and T_A with water vapour feedback at clear sky conditions. The respective climate sensitivity increases from C_S = *1.11* $^{\circ}C$ to *1.66* $^{\circ}C$ and the air sensitivity from A_S =*0.45* to *0.71* $^{\circ}C$, giving an amplification factor, caused by water vapour feedback, for C_S of 1.5 and for A_S of 1.58.

At regular cloud cover of 66 %, however, C_S only increases from *0.55* $^{\circ}C$ to *0.65* $^{\circ}C$ and A_S from *0.19* $^{\circ}C$ to *0.23* $^{\circ}C$ corresponding to reinforcements of 1.19 and 1.22.

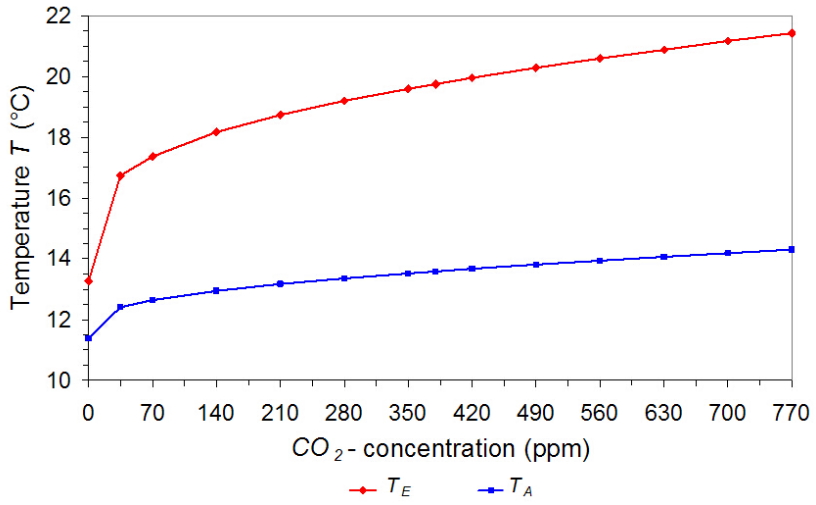

Figure 13. Calculated surface temperature T_E (red) and lower tropospheric temperature T_A (blue) as a function of CO_2 concentration with water vapour feedback at clear sky.

5.4.2 Lapse-Rate-Feedback

Under mean global conditions the average temperature decrease with altitude over the troposphere is specified as *6.5* $^{\circ}C/km$ and is assumed to be constant up to the tropopause at about *11 km* altitude [9]. As

already outlined in section 3 , this lapse rate has a direct influence on the power, which is asymmetrically re-radiated by the atmosphere in downward and upward direction. From radiation transfer calculations we find, that at this standard lapse rate the fraction radiated downward is f_A = *61.0 %,* and that rejected to space $(1 - f_A)$ = *39.0 %,* respectively. When this vertical temperature profile changes, it also induces a climatic effect, known as lapse rate feedback.

Global circulation models predict an enhanced warming in the upper troposphere of tropical regions, particularly in response to an increasing water vapour concentration. This would result in a negative feedback. On the other hand, at mid- to high-latitudes, a larger low level warming is expected as response to the positive radiative warming, thus, providing a positive feedback. Since the influence of the tropics is assumed to dominate, a resulting negative feedback of *-0.8* $Wm^{-2}K^{-1}$ ($\sim$ *-20 %*) is predicted [27, 28].

Independent of these effects we consider an additional slightly different influence of a changing lapse rate on the climate. It is well-known that the tropopause height is significantly varying from climate zone to climate zone (also over the seasons) and in so far is directly related to the local ground temperature. Whereas the mean absorption and re-radiation over a longer or shorter path in the troposphere will not noticeably be influenced, as long as the optical depth is almost constant, changes of the lapse rate in these climate zones with the ground temperature directly affect the asymmetry factor f_A and thus the total balance of *EASy*.

In the literature quite contradictory models can be found about the temperature distribution over the troposphere. So, one model assumes that due to convection the lapse rate over the troposphere is always constant and with a changing ground temperature the tropopause height is synchronously shifted up or down. The other extreme is to expect a constant height, at least within one climate zone, and to suppose that any ground temperature variations only affect the lapse rate.

From calculations with a fixed tropopause height over all zones and therefore a maximum lapse rate change from *7.5 °C/km* for the tropics (ground temperature: *26 °C*) to *4.5 °C/km* for the polar region (temperature: *-7 °C*), we derive a temperature dependence of the asymmetry factor of $df_A/dT_E = b_a$ = *0.145 % / °C* (see subsection 3.3, **Figure 8**). The reality obviously lies somewhere between these extremes, and it seems plausible to use a somewhat smaller value. Together with the predicted negative feedback, determined by the dominating tropical influence, we estimate a temperature dependence of:

$$\frac{df_A}{dT_E} = b_a = 0.05\ \%/^{\circ}C \tag{81}$$

For the respective sensitivities we then find C_S = *1.22 °C* and A_S = *0.6 °C*, which under regular cloud cover reduce to C_S = *0.62 °C* and A_S = *0.24 °C* .

Since the water vapour has a more or less stronger influence on the lapse rate, both effects are often considered together [27]. For the combined water vapour and lapse rate feedback we then get an amplification factor under clear sky conditions of 1.74 and with clouds of 1.37.

5.4.3 Earth Albedo Feedback

A further feedback results from the fact that with increasing ground temperature the Earth's reflectivity will be influenced, caused by the ice cover in the polar regions and changes of the vegetation. With varying reflectivity particularly the *sw* radiation balance will be modified in such a manner, that with

reducing reflectivity more power is absorbed by the Earth's surface which then contributes to an additional heating of the ground.

This Earth albedo influence is estimated as a positive feedback with an amplification between 10 and *15 %* [27, 28]. In our simulations we introduce this albedo feedback as a temperature dependent change of the Earth's reflectivity with:

$$\frac{dr_{SE}}{dT_E} = e_f = -0.17\ \%/^{\circ}C \tag{82}$$

which under clear sky contributes to an increase of the climate sensitivity of *15 %* and at mean overcast of *12 %*.

5.4.4 Convection Feedback

The sensible heat flux at the reference CO_2 concentration of *380 ppm* and temperature T_R = *16* $^{\circ}C$ (for clear sky *19.8* $^{\circ}C$) was chosen to be *17* W/m^2 in agreement with the TFK-scheme, and this flux was assumed to be constant in the previous simulations. From (76), however, we know that the heat transfer will generally be composed of two contributions, one constant part $I_{C0} = P_{C0}/A^Z$, determined by temperature independent processes for the heat transport at the boundary, and a second part, governed by the temperature difference between the surface and atmosphere with

$$I_C = P_C/A^Z = I_{C0} + {}^1\!/_4 h_C(T_E - T_A) \tag{83}$$

Due to the second term in this equation any temperature changes induced by CO_2, also initiate a feedback on *EASy*, which we may call convection feedback.

From **Figure 11** and **Figure 13** it can well be recognized that the air temperature reacts less sensitively to concentration variations than the Earth-temperature, and the difference $(T_E - T_A)$ increases with increasing CO_2 concentration. Therefore, also the sensible heat flux grows with the concentration. Since an increasing flux from the surface to the atmosphere contributes to an additional cooling, the resulting feedback will be negative.

The size of this feedback gets maximum, when the first term on the right side of (83) vanishes and the total heat flux of *17* W/m^2 at *380 ppm* CO_2 is determined by the second term. At clear sky and a temperature difference of $(T_E - T_A)$ = *6.2* $^{\circ}C$ then the heat convection coefficient can assume a maximum value of $h_{C,max}$ = *11* $W/m^2/^{\circ}C$, whereas under regular cloud cover with a temperature difference $(T_E - T_A)$ = *5.2* $^{\circ}C$ this maximum value is $h_{C,max}$ = *13* $W/m^2/^{\circ}C$. When choosing a smaller convection parameter, this automatically reduces the feedback but increases the first term in (83), so that at the reference CO_2 concentration always a sensible heat flux of *17* W/m^2 is guarantied.

For h_C = *10* $W/m^2/^{\circ}C$ for both cases, uncovered and covered, at clear sky we calculate a climate sensitivity of C_S = *0.96* $^{\circ}C$ corresponding to an attenuation of 0.86, and at regular cloud cover C_S = *0.45* $^{\circ}C$ with a reduction factor of 0.82. Sensible heat in this case consists of a constant contribution of *4* W/m^2 and a temperature dependent part of *13* W/m^2 at T_E = *16* $^{\circ}C$.

5.4.5 Evaporation Feedback

Similar to convection also evaporation of water and sublimation of ice contribute to cooling of the surface. Since an increasing Earth temperature further forces these processes, they also result in a negative feedback, which we call evaporation feedback. As already outlined in section 4, the latent heat flux may be expressed as:

$$I_L = P_L/A^Z = I_{L0} + l_H(T_E - T_0) \tag{84}$$

consisting of a temperature independent contribution I_{L0}, and a second term proportional to the ground temperature above the freezing point $(T_E - T_0)$. Under regular conditions I_{L0} almost vanishes, and the feedback, then only determined by the second term in (84), gets maximum. Since the total flux at the reference CO_2 concentration of $380\ ppm$ is held fixed to $80\ W/m^2$ in agreement with the TFK-scheme, at mean cloud cover the heat transfer coefficient l_H can assume a maximum value of $5\ W/m^2/\,^\circ C$ ($80\ W/m^2/16\,^\circ C$) and at clear sky $4\ W/m^2/\,^\circ C$ ($80\ W/m^2/19.8\,^\circ C$). When for some reason the heat transfer is less sensitively responding to temperature changes (*e.g.*, less rapidly increasing precipitation rate or saturating evaporation), l_H and by this the feedback may further be reduced. Then, in the same way, as the second term in (84) decreases, the first term increases.

Without clouds and maximum $l_H = 4\ W/m^2/\,^\circ C$ we find a climate sensitivity of $C_S = 0.72\,^\circ C$; at mean cloud cover and with $l_{H,max} = 5\ W/m^2/\,^\circ C$ it reduces to $C_S = 0.3\,^\circ C$, which corresponds to an attenuation by a factor of 0.56. So, latent heat can contribute to significant negative feedback.

In this context it should be noticed that generally evaporation and convection feedbacks are not mentioned or included in climate models considered by the *IPCC*, although obviously they have a quite strong influence on the adjusting temperature levels.

5.4.6 Thermally Induced Cloud Feedback

Comparison of the preceding simulations under clear sky and at cloudiness already demonstrates the dominant influence of the cloud cover on the self-adjusting equilibrium between the Earth and atmospheric layers. So, the climate sensitivity drops to about half its value compared to clear sky conditions, and the ground temperature approximately changes from *20* to $16\,^\circ C$, when the cloud cover increases from 0 to *66 %*. This temperature response was adopted from the *ISCCP*-observations of the global warming and mean cloud cover variations over the period *1983 - 2010* [25].

However, when for some reason the driving force for any of these observed changes is not the cloud cover but the temperature, acting back on the cloudiness, we have to consider an additional feedback process, which then further amplifies the *GH*-effect and even might overcompensate the previously observed reduction of sensitivities at cloudiness.

It is quite obvious that the registered temperature changes will not exclusively result from cloud variations or vice versa, but may also be influenced by variations of the solar radiation, the humidity or internal oscillations. In addition, also observations are known, particularly in the tropics, were just the opposite trend is found, that with increasing temperature also the cloud cover is increasing [29–32], which then contributes to negative feedback.

Therefore, obviously the worst case will be, to attribute any response of the cloud cover C_C, as derived from the *ISCCP*-data, only to the surface temperature change ΔT_E and to address this change only to the

CO_2-*GH*-effect, (CO_2 induced cloud feedback), this at least around the mean cloud cover of *66 %* and the mean global temperature of *16 ˚C*. Since even at very high temperatures clouds will not completely disappear, we suppose a rest cloudiness of $C_{C,min}$ = *20 %* and an exponential approach to this lower limit. Further, to represent the cloud cover also for negative ΔT_E's, as this is the case for smaller CO_2 concentrations than the reference at *380 ppm*, we use for reasons of uniqueness the same functional relation. So, we express the cloud cover as a function of the ground temperature by:

$$C_C(T_E) = \begin{cases} C_{C,\min} + (C_{CR} - C_{C,\min}) \cdot e^{-c_f (T_E - T_R)/T_R} & for\ T_E \geq T_R \\ C_{CR} \quad + (C_{CR} - C_{C,\min}) \cdot (1 - e^{c_f (T_E - T_R)/T_R}) & for\ T_E < T_R \end{cases} \tag{85}$$

with C_{CR} = *66 %* as the mean cloud cover at T_R = *16 ˚C* and c_f as the temperature induced cloud feedback parameter. In principle (85) just describes the reciprocal legality as used to derive the ground temperature variation as a function of the cloud cover. It is clear that for too large negative temperature deviations C_C would get larger than 100% and then has to be truncated, but within regular variations this is not the case.

To reproduce the cloud variations in agreement with the *ISCCP* observations, a feedback parameter of $c_f = 5.4$ is required, yielding a cloud cover change of *1 %* at ΔT_E = *0.065 ˚C*. A simulation with this value at mean cloud cover C_C = *66%* and assuming, that the cloud changes are only caused by the CO_2 *GH*-effect, this gives a climate sensitivity of C_S = *2.62 ˚C,* corresponding to an amplification of 4.8. On the other hand supposing a negative feedback of $c_f = -5.4$, the climate sensitivity would drop to C_S = *0.21 ˚C*. These examples already indicate, that for a reliable assessment of the climate sensitivity particularly reliable data about the driving force and size of any cloud cover changes are important, since they have an exceptionally strong influence on the further conclusions (see also Spencer and Braswell [33]).

5.4.7 Total Feedback

All results for the individual and collective feedbacks on the climate and air sensitivity are listed in **Table 7**. The upper ten rows show the data calculated under clear sky conditions, the lower 14 lines the results under mean cloud cover. Comparison of respective rows without and with overcast clearly demonstrates the dominant influence of clouds, causing a significant reduction of the sensitivities, as long as the thermally induced cloud feedback is excluded. So, with water vapour, lapse rate, albedo, convection and evaporation feedback C_S even diminishes to only *0.43 ˚C*.

Additionally assuming CO_2 induced cloud feedback with $c_f = 5.4$, the previously observed attenuation, compared to clear sky, is overcompensated and the climate sensitivity rises to C_S = *1.73 ˚C*, almost *60 %* larger than found for clear sky with *1.11 ˚C* (including the other feedbacks - see **Table 7**, line 10). The same mechanism, which reduces the temperature with increasing cloud cover, is also active in opposite direction, and this with the net result of an increased climate sensitivity. Under these conditions the observed warming over the last hundred twenty years of about *0.8 ˚C*, which the *IPCC* almost exclusively addresses to anthropogenic forcing, indeed might already be explained to 3/4 (*0.6 ˚C*) by the *100 ppm* CO_2 increase over this period, and the increased temperature altogether should have stimulated a reduced mean cloud cover of *11 %*.

Due to the above assumptions, that the observed cloud changes within the *ISCCP*-program are only thermally induced and the respective temperature increase over this period is only caused by CO_2, a climate sensitivity of C_S = *1.73 ˚C* obviously represents an upper limit for this quantity. Similar conclusions hold

Table 7. Calculated climate and air sensitivities at different feedback conditions.

Clouds $C_C(\%)$	c_f	water vapour	lapse rate $b_a(\%/^\circ C)$	albedo e_f $(\%/^\circ C)$	convection h_C $(W/m^2/^\circ C)$	evaporation l_H $(W/m^2/^\circ C)$	A_S $(^\circ C)$	C_S $(^\circ C)$	rel.
0	-	-	-	-	-	-	0.45	1.11	1.00
0	-	on	-	-	-	-	0.71	1.66	1.50
0	-	-	0.05	-	-	-	0.60	1.22	1.10
0	-	-	-	- 0.17	-	-	0.57	1.28	1.15
0	-	-	-	-	10	-	0.51	0.96	0.86
0	-	-	-	-	-	4	0.60	0.72	0.65
0	-	on	0.05	-	-	-	0.98	1.93	1.74
0	-	on	0.05	- 0.17	-	-	1.37	2.51	2.27
0	-	on	0.05	- 0.17	10	-	1.25	1.96	1.77
0	-	on	0.05	- 0.17	10	4	1.07	1.11	1.00
66	0	-	-	-	-	-	0.19	0.55	1.00
66	0	on	-	-	-	-	0.23	0.65	1.19
66	0	-	0.05	-	-	-	0.24	0.62	1.13
66	0	-	-	- 0.17	-	-	0.23	0.61	1.12
66	0	-	-	-	10	-	0.20	0.45	0.82
66	0	-	-	-	-	5	0.24	0.30	0.56
66	+5.4	-	-	-	-	-	1.67	2.62	4.77
66	-5.4	-	-	-	-	-	0.00	0.21	0.37
66	0	on	0.05	-	-	-	0.34	0.75	1.37
66	0	on	0.05	- 0.17	-	-	0.42	0.88	1.60
66	0	on	0.05	- 0.17	10	-	0.39	0.69	1.25
66	0	on	0.05	- 0.17	10	5	0.32	0.43	0.79
66	+5.4	on	0.05	- 0.17	10	5	2.09	1.73	3.14
66	-5.4	on	0.05	- 0.17	10	5	0.10	0.19	0.34

for the response of *EASy* with a ground temperature variation of *6.8* $^\circ C$ at a *100* % cloud cover change. In some way this is even confirmed by paleo-climate investigations [34], indicating that *EASy* obviously stabilizes itself within temperature variations of about *6 - 7* $^\circ C$, and this still under the influence of even much stronger solar changes as well as under $10x$ larger CO_2 concentrations, as they were found *500 Mio* years ago.

If the warming over the eighties and nineties additionally might have been superimposed by some other thermal processes, *e.g.*, an increased solar activity, Pacific Decadal Oscillations (*PDO*), the Southern Oscillation Index (*SOI*) or other *GH*-gases, the respective CO_2 initiated contribution to the cloud changes further diminishes and in the same way the climate sensitivity.

Altogether, we see that the dominating positive feedbacks, originating from clouds, water vapour, lapse rate and albedo, are partially compensated by evaporation and convection. Particularly clouds have two stronger ambivalent effects on the energy balance, which to some degree neutralize each other. However, which of them can dominate under special conditions, is still largely unknown [27, 28].

Up to now it is even not clear, if the *ISCCP* observations are really only a consequence of the increased temperature or at least to some degree are stimulated by a non-thermal solar activity over the observation period [35–41]. In the latter case the strong thermal cloud feedback had to be cancelled with the effect, that at otherwise same conditions the climate sensitivity would drop to less than *0.5* $^\circ C$.

An important criterion for any serious validation, which mechanism really might control the cloud cover changes, can be derived from model simulations, which additionally include any solar activity variations and compare these simulations directly with the observed global warming over the last century. Such kind of investigations have been performed by Ziskin and Shaviv [42] (see also [41], $p.95$), using an energy balance model with a diffusive deep ocean and additionally taking into account a non-thermal

solar component. They show that obviously such solar induced component is necessary to reproduce the *20th* century global warming and that the total solar contribution is much larger than can be expected from variations of the total solar irradiance (*TSI*) alone. Altogether they attribute *40 %* of global warming to the solar influence and *60 %* to anthropogenic activities.

To verify the existence and size of a solar effect in the total energy budget we have performed quite similar analyses, which also include solar variations and orientate at the observed warming over the last century, but which are based on our two-layer model, including all discussed feedback processes and especially reproducing the *ISCCP* observations of cloud cover changes. Of course, any conclusions deduced from such comparison sensitively depend on the reliability of the measured cloud cover, the solar activity and temperature changes over this period.

6. SIMULATIONS AND RESULTS WITH SOLAR INFLUENCE

In the same way as the *GH*-gases have an influence on the radiation and energy budget of *EASy*, this is the case for a varying solar activity. Both are external perturbations, causing an imbalance, to which *EASy* has to respond with a new distribution for the respective temperatures at the surface and in the atmosphere.

Such response on a varying solar activity can easily be simulated with the presented two-layer climate model by changing the solar constant (*Total Solar Irradiance - TSI*) in our parameter list in **Table 5**. So, a simulation with a *0.1 %* larger *TSI* contributes to an increase of the surface temperature of *0.09 ˚C*. In analogy to the CO_2 climate sensitivity we may call this the solar sensitivity S_S. Typically, over a Schwabe cycle (*11 years*) variations of the solar constant of *0.1 - 0.12 %* are observed, corresponding to an equilibrium temperature change of about *0.1 ˚C*.

6.1 Solar Induced Cloud Feedback

Since the amount of clouds varies over the solar cycle, there exists strong evidence that the solar activity variations also modulate the cloud cover. Actual publications of Svensmark [36–39] indicate, that with an increasing solar activity and, therefore, an increasing solar magnetic field the cosmic flux, which hits the atmosphere, is reduced and causes a direct feedback on the cloud cover. So, it is expected that the generation rate of aerosols as condensation seeds for the formation of water droplets in the lower atmosphere is directly influenced by the cosmic radiation flux (see also *CLOUD* experiment, [40]), which therewith also controls the cloud cover.

Another proposed mechanism is a hyper-sensitivity of the climate system to ultraviolet (*UV*) radiation, which typically varies $10x$ stronger over a solar cycle than the *TSI* [43–45]. So, increased *UV*-radiation activates the stratospheric ozone production and heat transfer, which via atmospheric waves can further induce sea surface temperature and/or tropospheric circulation variations and in this way also modulate the cloud cover [46].

Obviously both these mechanisms play a role, depending on the climatic conditions and altitude [47], but owing to their close interrelation they can only hardly be distinguished and here are further considered as a unique effect.

A reduced cloud formation at an increased solar activity then amplifies the initial *TSI* induced tem-

perature increase and can be included in the two-layer model as a feedback term (more precisely an amplification term) similar to the previous cloud feedback, but now depending on changes of the solar constant, supposing that variations in E_S initiate reciprocal changes in the cloud cover with:

$$C_C(E_S) = \begin{cases} C_{C,\min} + (C_{CR} - C_{C,\min}) \cdot e^{-s_f (E_S - E_{SR})/E_{SR}} & for\ E_S \geq E_{SR} \\ C_{CR} \quad + (C_{CR} - C_{C,\min}) \cdot (1 - e^{s_f (E_S - E_{SR})/E_{SR}}) & for\ E_S < E_{SR} \end{cases} \tag{86}$$

E_{SR} is the mean solar constant as a reference and s_f the solar induced cloud feedback parameter.

Assuming, that the cloud cover variation over the period *1983 - 2000* of *-4 %* is only determined by an observed increase of the *TSI* of $\delta E_S = 0.1$ % [35], this results in a feedback parameter $s_f = 90$.

With this additional solar induced cloud feedback the solar sensitivity rises to $S_S = 0.38\ ^\circ C$. However, in the same way as any warming causes further feedback processes, as discussed in sub-section 5.4, they also further amplify or attenuate such solar induced temperature changes with one exception, that now the temperature induced cloud feedback is replaced by the solar induced cloud effect.

The calculations including all the other feedbacks are listed in **Table 8**. They even show a slightly decreasing sensitivity of $S_S = 0.32\ ^\circ C$ (see line 3), which is due to the influence of convection and evaporation.

Table 8. Calculated solar sensitivity at different feedback conditions.

C_C at 66 % c_f	s_f	water vapour	lapse rate b_a(%/°C)	albedo e_f (%/°C)	convection h_C ($W/m^2/^\circ C$)	evaporation l_H ($W/m^2/^\circ C$)	S_S (ΔE_S=0.1%) (°C)	rel.
-	0	-	-	-	-	-	0.09	1.00
-	90	-	-	-	-	-	0.38	4.35
-	90	on	0.05	-0.17	10	5	0.32	3.65
5.4	-	on	0.05	-0.17	10	5	0.44	5.01

When solar induced cloud feedback is the only responsible process controlling the cloud cover, also for the CO_2 climate sensitivity the temperature induced cloud feedback has to be cancelled and C_S reduces to $0.43\ ^\circ C$ (see **Table 7**, line 22).

An analysis of Shapiro *et al.* [48] of long-term solar activity proxies over the last century shows an increase of the *TSI* of about $\Delta E_S = 0.2$ %. Such an increase is in good agreement with the observed decadal group sunspot numbers over this period (see, *e.g.*, Hoyt and Schatten [49]) and is remarkably well confirmed by a new adjustment-free physical reconstruction of solar activities (Usoskin *et. al.* [50]), indicating a modern Grand maximum (during solar cycles 19–23, *i.e.*, 1950–2009), which was found to be a rare or even unique event, in both magnitude and duration, in the past three millennia.

With a solar sensitivity of $S_S = 0.32\ ^\circ C$ and an increase of $\Delta E_S = 0.2$ % this already results in a temperature rise of $0.64\ ^\circ C$, whereas CO_2 with an increase of *100 ppm* over this period (and applying the respective climate sensitivity of $C_S = 0.43\ ^\circ C$), only delivers additional $0.1\ ^\circ C$. Together, both contributions already explain very well the measured temperature growth of $0.74\ ^\circ C$ over the last 120 years [51]. Additional contributions possibly stimulated by *PDO* or *SOI* have been neglected. Under these conditions the influence of the sun on global warming would even be 6*x* larger than the greenhouse effect.

Actually, a quite strong correlation between solar activities and the Earth's temperature changes is also reported by Zhao and Feng [52], who have investigated the periodicities of the solar activity and the Earth's temperature variation on a time scale of centuries, using the wavelet and cross correlation

analysis techniques. From this they conclude, that during the past 100 years solar activities display a clear increasing tendency which corresponds very well with the global warming of the Earth (including land and ocean).

If the solar anomaly (related to the last century) should have been overestimated and would only be $\Delta E_S = 0.1$ %, the solar fraction still yields the dominant part. In this case the global warming balance could further be satisfied, *e.g.*, reducing the negative evaporation and convection feedbacks to $l_H = h_C = 0.8\ W/m^2/^\circ C$. Then the sun still would contribute $0.51\ ^\circ C$ and CO_2 $0.23\ ^\circ C$ to global warming.

It should be noticed, that as long as the solar influence is considered to be the responsible mechanism of the cloud cover change over the period *1983 - 2000* and this change is not impeached, a smaller assumed increase of the *TSI* over this period (hereafter designated as δE_S), and therefore deviating from Ref. 35, only pushes the parameter s_f further up and increases the solar feedback.

We do not discuss any additional influence of aerosols over this period, since any reliable figure of such effect is largely unknown. Implicitly aerosols are already enclosed in our model via atmospheric and cloud backscattering, so that any aerosol impact could easily be modelled by varying the *sw* backscattering parameters, and if necessary also the cloud absorption.

6.2 Thermally Induced Cloud Feedback

If any non-thermal solar induced cloud feedback is denied and only thermally induced cloud variations are considered, then this feedback also has to be applied to the direct solar initiated warming. We further focus only on CO_2- and solar-induced contributions, while other effects are neglected. For the climate and solar sensitivity this rather gives an upper limit. Their individual contributions and, therefore, their relative weighting might be derived, comparing the non-amplified CO_2 fraction with the respective solar part. For *100 ppm* CO_2 increase this gives $0.19\ ^\circ C$ and for a solar anomaly of $\Delta E_S = 0.2\%$ then $0.18\ ^\circ C$. Therefore, the relative contributions are 0.52 and 0.48. However, different feedbacks are acting slightly different on both contributions, so it is more appropriate to compare the amplified fractions.

With a feedback parameter $c_f = 5.4$ and, therefore, in agreement with the observed cloud variations, then the solar sensitivity even increases to $S_S = 0.44\ ^\circ C$ (see **Table 8**), and with an *TSI*-anomaly of $\Delta E_S = 0.2$ % this already would contribute to a solar stimulated temperature increase of $0.72\ ^\circ C$ (slightly nonlinear increase with ΔE_S). In this case CO_2 delivers an additional contribution of $0.6\ ^\circ C$ (corresponding to a climate sensitivity of $C_S = 1.73\ ^\circ C$). Together this is almost twice the observed temperature boost over the last 120 years. Even with a reduced anomaly of only $\Delta E_S = 0.1$ % the calculated warming with $1.04\ ^\circ C$ would still be too large and could only further be pushed down by significantly reducing other feedback parameters.

Well knowing, that the observed warming does not represent an equilibrium state - different to our calculations -and can further be superimposed by other effects like the *PDO* and *SOI* [33, 42], which even could increase the discrepancy, it is quite obvious that such large thermal cloud feedback is unrealistically high. With a reduced feedback the temperature balance could again be satisfied, *e.g.*, with $c_f = 4.0$ and maximum feedback parameters for convection and evaporation, or with more moderate values for $c_f = 3.5$ and $h_C = l_H = 4\ W/m^2/^\circ C$. In both cases CO_2 would contribute $0.33\ ^\circ C$ and the sun (without solar-induced cloud cover feedback) $0.41\ ^\circ C$. But such reduced thermal feedback then is no longer in agreement with the observed cloud changes. As a consequence, the measured cloud cover change by the *ISCCP* cannot exclusively be explained by global warming, but at least some fraction must also be

attributed to the solar-induced cloud cover changes.

6.3 Combined Thermal- and Solar-Induced Feedback

From the preceding discussion we see that any reliable specification of the climate and solar sensitivity requires a deeper understanding of the mechanisms and contributions, controlling the cloud cover and this in combination with further verified proxies of the solar activity. So, it still exists some controversy, whether the solar anomaly deduced by Shapiro *et al.* [48] is overestimated or not (see also Wenzler *et al.* [53]). As long as no more reliable data are available, we distinguish between two scenarios for $\Delta E_S = 0.2$ % and *0.1* % over the last century.

To achieve consistency in our fits with the observed global warming and also with the measured cloud cover variation, we apply as a further extension of our model a combination of the thermally and solar induced cloud feedbacks, where the weighting of these mechanisms is determined to satisfy both constraints. This can be performed with varying feedback parameters, which then determine the weighting of a mechanism relative to their maximum values, or with fixed (maximum) parameters and then directly weighting the two feedback processes in agreement with the constraints. Both procedures give similar results, but the second appears more straight-forward and was preferred in our simulations.

The main results together with respective parameters for these calculations are compiled in **Table 9**. Water vapour, lapse rate and albedo feedbacks are included but not additionally listed up.

Table 9. Calculated solar and climate sensitivity at combined thermally and solar induced cloud feedback.

weighting (%)		$\Delta E_S(\%)$	$\delta E_S(\%)$	c_f	s_f	convec. h_C	evapor.	$S_S(^\circ C)$	$C_S(^\circ C)$
therm.	solar					$(W/m^2/^\circ C)$	$l_H(W/m^2/^\circ C)$		
0	100	0.2	0.1	0	90	10	5	0.32	0.43
51	49	0.1	0.1	5.4	90	10	5	0.36	1.09
32	68	0.1	0.1	5.4	90	4	4	0.40	0.95
9	91	0.1	0.05	5.4	180	4	4	0.54	0.56

As already outlined above, for the case of $\Delta E_S = 0.2$ % excellent agreement can already be found, only considering solar-induced cloud cover feedback. With a convection coefficient $h_C = 10\ W/m^2/^\circ C$ and an evaporation parameter of $l_H = 5\ W/m^2/^\circ C$ then the solar contribution accounts for *0.64* $^\circ C$ and CO_2 only for *0.1* $^\circ C$, yielding a solar sensitivity of S_S = *0.32* $^\circ C$ and a climate sensitivity of C_S = *0.43* $^\circ C$.

When supposing an *TSI*-anomaly over the last century of only $\Delta E_S = 0.1\%$ at otherwise same conditions, we only get consistency with the observed global warming and cloud cover changes for a thermal to solar fraction of *51/49* %, (c_f = *5.4*, $s_f = 90$) yielding a CO_2 contribution of *0.38* $^\circ C$ to global warming. With more moderate parameters $h_C = l_H = 4\ W/m^2/^\circ C$ we find a ratio *32/68* % with a CO_2 contribution of *0.34* $^\circ C$ and a solar part of *0.40* $^\circ C$, resulting in a solar sensitivity of *0.40* $^\circ C$ and a climate sensitivity of *0.95* $^\circ C$.

These examples for stronger or more moderate convection and evaporation feedbacks show, that this has no bigger influence on the final result. In order to fit the global warming, smaller feedbacks for sensible and latent heat are just compensated by a different weighting of the thermal to solar cloud cover feedback with relatively small changes in the respective solar or CO_2 contributions (about *10%*). This means, even when h_C and l_H are not accurately known, this does not affect too much the overall-reliability of such fitting procedure.

However, when assuming a reduced *TSI*-anomaly of $\Delta E_S = 0.1\%$ over the last century, it appears consequent, also to emanate from a smaller solar variation δE_S over the period *1983 - 2000*. As already stated before, this results in a larger feedback parameter s_f, which at an increase of only $\delta E_S = 0.05$ % over this time interval rises up to $s_f = 180$ to further explain the observed cloud variation. A fit under these conditions and with $h_C = l_H = 4\ W/m^2/\,^\circ C$ gives a weighting for the thermal to solar cloud feedback of *9/91 %* with a solar fraction of *0.54* $^\circ C$ and a CO_2 initiated contribution of *0.2* $^\circ C$. The first part just reflects the solar sensitivity, whereas for the equilibrium climate sensitivity we calculate $C_S = 0.56\,^\circ C$, which under the above assumptions of a relatively small solar anomaly rather represents an upper limit for this quantity. The respective plot of the temperatures T_E and T_A as a function of the CO_2 concentration is shown in **Figure 14**. In this case both graphs almost proceed parallel to each other, so that convection only contributes to small (and under these conditions even slightly positive) feedback.

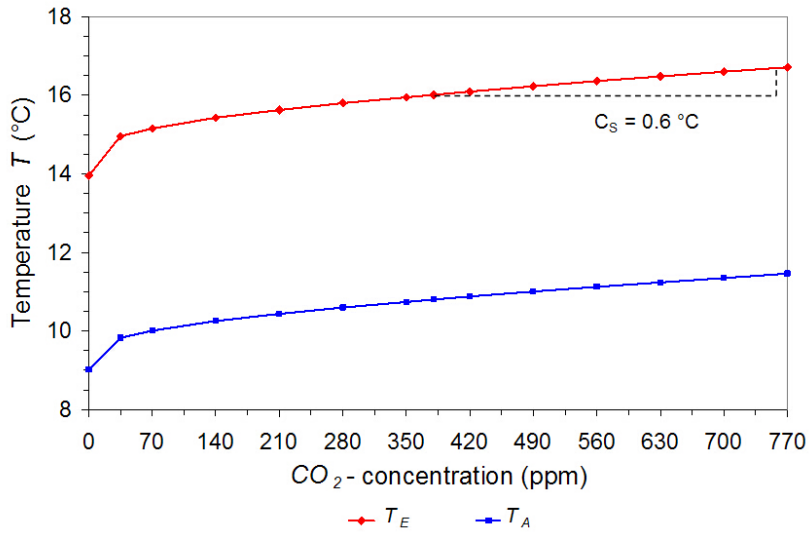

Figure 14. Calculated surface temperature T_E (red) and lower tropospheric temperature T_A (blue) as a function of CO_2 concentration, based on a combination of thermally and solar induced cloud feedback.

6.4 Assessment of Results

We find that in all scenarios, which include solar activities, this solar contribution to global warming is the dominant part and under special conditions could even be up to 6*x* larger than the CO_2 influence. This is in clear contradiction to the *IPCC*, which traces the rising temperatures over the last century back to the anthropogenic emission of *GH*-gases (*95 %* probability), whereas any noticeable solar effect is denied. Our calculations show, that the solar part can only be pushed below the greenhouse contribution, when the increase of the *TSI* over the last century is assumed to be smaller than *0.1 %* and almost identical with the variations over the period *1983 - 2000* ($\Delta E_S \approx \delta E_S$).

Of course, no solar influence would exist, when any solar anomaly could completely be excluded, this over the *20th* century as well as over the eighties and nineties in contradiction to Refs [35, 42, 48–50, 52]. Then the worst case with respect to global warming by CO_2 would be, to attribute the observed *ISCCP* cloud changes only to CO_2 induced thermal feedback and to exclude all other influences like the *PDO, SOI* or other *GH*-gases. For this special and rather improbable scenario we calculate a maximum climate

sensitivity of $C_S = 1.73\,^{\circ}C$ (see **Table 7**, line 23), explaining $0.6\,^{\circ}C$ of the warming over the last century. In spite of the maximum thermally induced cloud feedback this sensitivity still lies at the lower edge of the *IPCC* data range [1], this because of the smaller water vapour feedback we deduce here, and the inclusion of two additional processes, the convection and evaporation feedback, which are generally not considered in the *IPCC* publications.

Additionally including solar activities over the last century as well as all relevant feedback processes, we derive with a lower anomaly of $\Delta E_S = 0.1\%$ a solar sensitivity of $S_S = 0.5\,^{\circ}C$ and a climate sensitivity of $C_S = 0.6\,^{\circ}C$, which are in full agreement with all constraints. Supposing a larger anomaly of $\Delta E_S = 0.2\%$ the respective sensitivities would still further decline to $S_S = 0.3\,^{\circ}C$ and $C_S = 0.4\,^{\circ}C$.

The largest uncertainties in all these considerations result from the cloud feedback mechanisms, and the solar variations, which are estimated to be *50 %*.

In principle our calculations confirm the investigations of Ziskin and Shaviv [42], showing the basically strong influence of solar activities on the climate. The higher solar and therefore smaller CO_2 contribution in our case may be attributed to the fact that we use different feedback contributions and also additional feedback processes, which for the climate sensitivity are deduced from our own calculations and for the solar sensitivity are essentially orientated at the cloud changes in the eighties and nineties. In addition, our calculations only represent an equilibrium state of *EASy*, whereas Ziskin *et al.* derive their data from a multidimensional fit to the temperature evolution over the last century.

In any case, the preceding discussion makes clear, that a climate sensitivity in agreement with the *IPCC* data [1] would only be possible, when any solar induced influence could be completely denied and a strong CO_2 induced thermal cloud feedback would be assumed.

7. CONCLUSION

The objective of this paper was to examine and to quantify the influence of *GH*-gases on our climate. Based on the *HITRAN-2008* database [4] detailed spectroscopic calculations on the absorptivities of water vapour and the gases carbon dioxide, methane and ozone in the atmosphere are presented.

The line-by-line calculations for solar radiation from $0.1–8\ \mu m$ (*sw* radiation) as well as for the terrestrial radiation from $3–100\ \mu m$ (*lw* radiation) show, that due to the strong overlap of the CO_2 and CH_4 spectra with water vapour lines the influence of these gases significantly declines with increasing water vapour pressure, and that with increasing CO_2-concentration well noticeable saturation effects are observed limiting substantially the impact of CO_2 on global warming.

The calculations were performed for three climate zones, the tropics, mid-latitudes and high-latitudes, based on actual data of the water vapour content, which is considerably varying with altitude above ground as well as with the climate zone and, therefore, with the temperature. The vertical variation in humidity and temperature as well as in the partial gas pressures and the total pressure is considered by computing individual absorption spectra for up to 228 atmospheric layers and then integrating from ground level up to *86 km* altitude.

The varying path length of sun light in these layers, which depends on the angle of incidence to the atmosphere and therefore on the geographic latitude and longitude, is included by considering the Earth as a truncated icosahedron (Bucky ball) consisting of 32 surface elements with well defined angles to the incident radiation, and assigning each of these areas to one of the three climate zones.

Propagation of the long-wave radiation, in particular the up- and down-welling radiation, emitted by the atmosphere itself, as well as their variation with temperature are derived from radiation transfer calculations for each zone.

To identify the influence of the absorbing gases on the climate and particularly the effect of an increasing CO_2-concentration on global warming, we developed an advanced two-layer climate model, which describes the Earth's surface and the atmosphere as two layers acting simultaneously as absorbers and Planck radiators. Also heat transfer by convection and evaporation between these layers is considered. At equilibrium each, the surface as well as the atmosphere, deliver as much power as they suck up from the sun and the neighbouring layer or climate zone.

The model includes *sw* and *lw* scattering processes at the atmosphere and at clouds, in particular considering multiple scattering between the surface and clouds. It also includes the common feedback processes like water vapour, lapse rate and albedo feedback, but additionally takes into account the influence of a temperature dependent sensible and latent heat flux as well as temperature induced and solar induced cloud cover feedback.

As direct reference for the incident and outgoing fluxes in the model we use the energy and radiation budget scheme of Tremberth et al. [20], which at a reference CO_2 concentration of *380 ppm* and a ground temperature of $16\,^{\circ}C$ can well be reproduced.

With the *sw* and *lw* absorptivities as the key parameters in such model then the surface temperature and the lower atmospheric temperature are calculated as a function of the CO_2 concentration. From the temperature variations, found at doubled CO_2 concentration, the CO_2 climate sensitivity and air sensitivity are derived.

Particularly the individual feedback processes with their different influence on the climate sensitivity are extensively discussed. While the albedo- and to some degree the lapse rate feedback are adopted from literature, the water vapour feedback is derived from the *sw* and *lw* absorptivity calculations over the different climate zones. With an amplification at clear sky conditions of 1.5 and at mean cloud cover of 1.2 these values are smaller than assumed in other climate models [27, 28].

Since it is found that with increasing CO_2 concentration the air temperature is less rapidly increasing than the surface temperature, the convection at the boundary of both layers rises with the concentration. As a consequence more thermal energy is transferred from the surface to the atmosphere. Similarly, with increasing temperature also evaporation and precipitation are increasing with the ground temperature. Both these effects contribute to negative feedback and are additionally included in the simulations.

A special situation is found for the influence of clouds on the radiation and energy budget. From measurements of the global cloud cover over a period of 27 years it is deduced that the global mean temperature is increasing with decreasing cloud cover [25]. However, it is not clear, if a lower cloud cover is the consequence of the increasing temperature, or if the cloud cover is influenced and at least to some degree controlled by some other mechanism, particularly solar activities. In the first case a strong amplifying temperature induced cloud feedback had to be considered, this for the climate sensitivity as well as for a respective solar sensitivity, whereas in the other case the temperature induced cloud effect would disappear for both sensitivities and only a solar induced cloud feedback had to be included due to the solar influence.

A deliberate approach which mechanism really controls the cloud cover with its dominant influence on the climate and solar sensitivity can be derived from model simulations, which additionally include the solar effect and compare this with the measured temperature increase over the last century. These

simulations, considering both effects, show that the observed global warming of *0.74 ˚C* [51] can only satisfactorily be explained, when a temperature feedback on the clouds is completely excluded or only has a minor influence. Otherwise the calculated warming would be significantly larger than observed, or the thermally induced cloud feedback would have been overestimated. With a combination of temperature and solar induced cloud feedback we deduce a CO_2 climate sensitivity of $C_S = 0.6$ ˚*C* and a solar sensitivity, related to *0.1 %* change of the solar constant, of $S_S = 0.5$ ˚*C*. An increase in the solar activity of only *0.1 %* over 100 years then contributes to a warming of *0.54 ˚C*, and the *100 ppm* increase of CO_2 over this period causes additional *0.2 ˚C* in excellent agreement with the measured warming and cloud cover.

From our investigations, which are based on actual spectroscopic data and which consider all relevant feedback processes as well as the solar influence, we can conclude, that a CO_2 climate sensitivity larger *1 ˚C* seems quite improbable, whereas a value of *0.5 - 0.7 ˚C* - depending on the considered solar anomaly - fits well with all observations of a changing solar constant, the cloud cover and global temperature. A climate sensitivity in agreement with the *IPCC* specifications (*1.5 - 4.5 ˚C*) would only be possible, when any solar influence could completely be excluded, and only CO_2 induced thermal cloud feedback would be assumed, then yielding a value of *1.7 ˚C*.

It should be noticed that different to general circulation models, which try to predict local climate variations over some time period and, therefore, have to solve complex coupled nonlinear differential equations with countless parameters, for tracing the climate sensitivity this is of no significance. We calculate an equilibrium state and can average over larger local variations, for which a partitioning into three climate zones is quite sufficient. In addition, a simple energy balance model, focussing on the main physical processes, is much more transparent than any *AOGCM* and can help to better understand the complex interrelations characterizing our climate system.

References

[1] IPCC, "Summary for Policymakers," *Climate Change 2013: The Physical Science Basis. Contribution of Working Group I to the Fifth Assessment Report of the Intergovernmental Panel on Climate Change [T.F. Stocker, D. Qin, G.-K. Plattner, M. Tignor, S.K. Allen, J. Boschung, A. Nauels, Y. Xia, V. Bex and P.M. Midgley (eds.)]. Cambridge University Press, Cambridge, United Kingdom and New York, NY, USA*, 2013.

[2] D. Randall, R. Wood, S. Bony, R. Colman, T. Fichefet, J. Fyfe, V. Kattsov, A. Pitman, J. Shukla, J. Srinivasan, *et al.*, "Climate Models and Their Evaluation," *Climate Change 2007: The Physical Science Basis. Contribution of Working Group I to the Fourth Assessment Report of the Intergovernmental Panel on Climate Change [Solomon, S., D. Qin, M. Manning, Z. Chen, M. Marquis, K.B. Averyt, M.Tignor and H.L. Miller (eds.)]. Cambridge University Press, Cambridge, United Kingdom and New York, NY, USA*, 2007.

[3] IPCC, "Climate Change 2001: The Scientific Basis," *Contribution of Working Group 1 to the Third Assessment Report of the Intergovernmental Panel on Climate Change, edited by J. T. Houghton, Y. Ding, D. J. Griggs, M. Noguer, P. J. van der Linden, X. Dai, K. Maskell and C. A. Johnson (eds). Cambridge University Press, Cambridge, UK, and New York, USA, chapter 6: Radiative Forcing of Climate Change*, p. 354, 2001.

[4] L. S. Rothman, I. E. Gordon, A. Barbe, D. C. Benner, P. F. Bernath, M. Birk, V. Boudon, L. R. Brown, A. Campargue, J.-P. Champion, *et al.*, "The HITRAN 2008 molecular spectroscopic database," *Journal of Quantitative Spectroscopy and Radiative Transfer*, vol. 110, no. 9, pp. 533–572, 2009.

[5] R. M. Goody and Y. L. Yung, *Atmospheric Radiation: Theoretical Basis, 2nd ed.* New York, NY: Oxford University Press, 1989.

[6] M. L. Salby, *Physics of the Atmosphere and Climate*. Cambridge University Press, 2012.

[7] H. Harde, "Radiation and Heat Transfer in the Atmosphere: A Comprehensive Approach on a Molecular Basis," *International Journal of Atmospheric Sciences*, vol. 2013. http://dx.doi.org/10.1155/2013/503727.

[8] L. S. Rothman, C. Rinsland, A. Goldman, S. Massie, D. Edwards, J. Flaud, A. Perrin, C. Camy-Peyret, V. Dana, J.-Y. Mandin, *et al.*, "The HITRAN Molecular Spectroscopic Database and HAWKS; 1996 Edition," *Journal of Quantitative Spectroscopy and Radiative Transfer*, vol. 60, no. 5, pp. 665–710, 1998.

[9] US Standard Atmosphere, "National Oceanic and Atmospheric Administration, National Aeronautics and Space Administration," tech. rep., Washington D.C., 1976.

[10] S. Vey, *Bestimmung und Analyse des atmosphärischen Wasserdampfgehaltes aus globalen GPS-Beobachtungen einer Dekade mit besonderem Blick auf die Antarktis*. PhD thesis, Technical University Dresden, 2007.

[11] H. Harde, *Was trägt CO_2 wirklich zur globalen Erwärmung bei? Spektroskopische Untersuchungen und Modellrechnungen zum Einfluss von H_2O, CO_2, CH_4 und O_3 auf unser Klima*. Books on Demand, Norderstedt, 2011. ISBN: 9 783842 371576.

[12] H. Harde and J. Pfuhl, "MolExplorer A Program-Platform for the Calculation of Molecular Spectra and Radiation Transfer in the Atmosphere," 2006–2014.

[13] K. Schwarzschild, "Göttinger Nachrichten," p. 41, 1906.

[14] R. Hanel, B. Conrath, V. Kunde, C. Prabhakara, I. Revah, V. Salomonson, and G. Wolford, "The Nimbus 4 Infrared Spectroscopy Experiment, 1. Calibrated Thermal Emission Spectra," *Journal of Geophysical Research*, vol. 77, no. 15, pp. 2629–2641, 1972.

[15] B. Barkstrom, E. Harrison, G. Smith, R. Green, J. Kibler, R. Cess, and the ERBE Science Team, "Earth Radiation Budget Experiment(ERBE) archival and April 1985 results," *Bulletin of the American Meteorological Society*, vol. 70, no. 10, pp. 1254–1262, 1989.

[16] T. D. Bess and G. L. Smith, "Earth radiation budget: Results of outgoing longwave radiation from Nimbus-7, NOAA-9, and ERBS satellites," *Journal of Applied Meteorology*, vol. 32, no. 5, pp. 813–824, 1993.

[17] B. A. Wielicki, B. R. Barkstrom, E. F. Harrison, R. B. Lee III, G. Louis Smith, and J. E. Cooper, "Clouds and the Earth's Radiant Energy System (CERES): An earth observing system experiment," *Bulletin of the American Meteorological Society*, vol. 77, no. 5, pp. 853–868, 1996.

[18] B. A. Wielicki, K. Priestley, P. Minnis, N. Loeb, D. Kratz, T. Charlock, D. Doelling, and D. Young, "CERES radiation budget accuracy overview," in *Preprints, 12th Conf. on Atmospheric Radiation, Madison, WI, Amer. Meteor. Soc*, vol. 9, 2006.

[19] T. Wong, B. A. Wielicki, R. B. Lee III, G. L. Smith, K. A. Bush, and J. K. Willis, "Re-examination of the observed decadal variability of Earth Radiation Budget using altitude-corrected ERBE/ERBS nonscanner WFOV data," *Journal of Climate*, vol. 19, no. 16, pp. 4028–4040, 2006.

[20] K. E. Trenberth, J. T. Fasullo, and J. Kiehl, "Earths Global Energy Budget," *Bulletin of the American Meteorological Society*, vol. 90, no. 3, pp. 311–323, 2009.

[21] D. D. Turner, E. J. Mlawer, G. Bianchini, M. P. Cadeddu, S. Crewell, J. S. Delamere, R. O. Knuteson, G. Maschwitz, M. Mlynzcak, S. Paine, *et al.*, "Ground-based high spectral resolution observations of the entire terrestrial spectrum under extremely dry conditions," *Geophysical Research Letters*, vol. 39, no. 10, 2012.

[22] W. Dines, "The heat balance of the atmosphere," *Quarterly Journal of the Royal Meteorological Society*, vol. 43, no. 182, pp. 151–158, 1917.

[23] K. N. Liou, *An Introduction to Atmospheric Radiation, 2nd ed*, vol. 84. Academic Press, San Diego, CA, 2002.

[24] R. Link and H.-J. Lüdecke, "A new basic 1-dimensional 1-layer model obtains excellent agreement with the observed Earth temperature," *Int. J. Modern Physics C*, vol. 22, pp. 449–455, 2011.

[25] International Satellite Cloud Climatology Project(ISCCP) http://isccp.giss.nasa.gov/products/onlineData.html or http://www.climate4you.com/index.htm.

[26] D. L. Hartmann, *Global Physical Climatology*, vol. 56. Academic Press, New York, 1994.

[27] Reference 2, section 8.6.3. http://www.ipcc.ch/publications_and_data/ar4/wg1/en/ch8s8-6-3-1.html.

[28] B. J. Soden and I. M. Held, "An assessment of climate feedbacks in coupled ocean-atmosphere models," *Journal of Climate*, vol. 19, no. 14, pp. 3354–3360, 2006.

[29] R. S. Lindzen, M.-D. Chou, and A. Y. Hou, "Does the Earth have an adaptative infrared iris?," *Bulletin of the American Meteorological Society*, vol. 82, no. 3, pp. 417–432, 2001.

[30] B. A. Laken and E. Pallé, "Understanding sudden changes in cloud amount: The Southern Annular Mode and South American weather fluctuations," *Journal of Geophysical Research: Atmospheres*, vol. 117, no. D13, pp. 1984–2012, 2012.

[31] H. Cho, C.-H. Ho, and Y.-S. Choi, "The observed variation in cloud-induced longwave radiation in response to sea surface temperature over the Pacific warm pool from MTSAT-1R imagery," *Geophysical Research Letters*, vol. 39, no. 18, 2012.

[32] P. M. Caldwell, Y. Zhang, and S. A. Klein, "CMIP3 Subtropical Stratocumulus Cloud Feedback Interpreted Through a Mixed-Layer Model," *Journal of Climate*, 2012.

[33] R. W. Spencer and W. D. Braswell, "On the Misdiagnosis on Surface Temperature Feedbacks from Variations in Earth's Radiant Energy Balance," *Remote Sensing*, vol. 3, no. 8, pp. 1603–1613, 2011.

[34] J.-R. Petit, J. Jouzel, D. Raynaud, N. I. Barkov, J.-M. Barnola, I. Basile, M. Bender, J. Chappellaz, M. Davis, G. Delaygue, *et al.*, "Climate and Atmospheric History of the past 420,000 Years from the Vostok Ice Core, Antarctica," *Nature*, vol. 399, no. 6735, pp. 429–436, 1999.

[35] R. C. Willson and A. V. Mordvinov, "Secular Total Solar Irradiance Trend During Solar Cycles 21 - 23," *Geophysical Research Letters*, vol. 30, no. 5, pp. 1–4, 2003.

[36] H. Svensmark, "Influence of Cosmic Rays on Earth's Climate," *Physical Review Letters*, vol. 81, no. 22, pp. 5027–5030, 1998.

[37] H. Svensmark, J. O. P. Pedersen, N. D. Marsh, M. B. Enghoff, and U. I. Uggerhøj, "Experimental Evidence for the Role of Ions in Particle Nucleation under Atmospheric Conditions," *Proceedings of the Royal Society A: Mathematical, Physical and Engineering Science*, vol. 463, no. 2078, pp. 385–396, 2007.

[38] H. Svensmark, T. Bondo, and J. Svensmark, "Cosmic Ray Decreases affect Atmospheric Aerosols and Clouds," *Geophysical Research Letters*, vol. 36, no. 15, pp. 1–4, 2009.

[39] M. B. Enghoff, J. O. P. Pedersen, U. I. Uggerhøj, S. M. Paling, and H. Svensmark, "Aerosol Nucleation Induced by a High Energy Particle Beam," *Geophysical Research Letters*, vol. 38, no. 9, pp. 1–4, 2011.

[40] J. Kirkby, J. Curtius, J. Almeida, E. Dunne, J. Duplissy, S. Ehrhart, A. Franchin, S. Gagné, L. Ickes, A. Kürten, *et al.*, "Role of Sulphuric Acid, Ammonia and Galactic Cosmic Rays in Atmospheric Aerosol Nucleation," *Nature*, vol. 476, no. 7361, pp. 429–435, 2011.

[41] F. Vahrenholt and S. Lüning, *Die kalte Sonne*. Hoffmann und Campe Verlag, Hamburg, 2012.

[42] S. Ziskin and N. J. Shaviv, "Quantifying the role of solar radiative forcing over the 20th century," *Advances in Space Research*, vol. 50, no. 6, pp. 762–776, 2012.

[43] J. D. Haigh, "The role of stratospheric ozone in modulating the solar radiative forcing of climate," *Nature*, vol. 370, no. 6490, pp. 544–546, 1994.

[44] J. D. Haigh, "The impact of solar variability on climate," *Science*, vol. 272, no. 5264, pp. 981–984, 1996.

[45] J. D. Haigh, A. R. Winning, R. Toumi, and J. W. Harder, "An influence of solar spectral variations on radiative forcing of climate," *Nature*, vol. 467, no. 7316, pp. 696–699, 2010.

[46] J. Kristjánsson, J. Kristiansen, and E. Kaas, "Solar activity, cosmic rays, clouds and climate: An update," *Advances in Space Research*, vol. 34, no. 2, pp. 407–415, 2004.

[47] M. Voiculescu, I. G. Usoskin, and K. Mursula, "Different response of clouds to solar input," *Geophysical Research Letters*, vol. 33, no. 21, 2006.

[48] A. Shapiro, W. Schmutz, E. Rozanov, M. Schoell, M. Haberreiter, A. Shapiro, and S. Nyeki, "A New Approach to Long-Term Reconstruction of the Solar Irradiance Leads to Large Historical Solar Forcing," *Astronomy & Astrophysics,*, vol. 529, pp. 1–8, 2011.

[49] D. V. Hoyt and K. H. Schatten, "Group Sunspot Numbers: A new solar activity reconstruction," *Solar Physics*, vol. 179, p. 189, 1998.

[50] I. Usoskin, G. Hulot, Y. Gallet, R. Roth, A. Licht, F. Joos, G. Kovaltsov, E. Thébault, and A. Khokhlov, "Evidence for distinct modes of solar activity," *Astronomy & Astrophysics*, vol. 562, 2014.

[51] Goddard Institute for Space Studies. http://data.giss.nasa.gov/gistemp/graphs.

[52] X. ZHAO and X. FENG, "Periodicities of solar activity and the surface temperature variation of the Earth and their correlations," *Chinese Science Bulletin*, vol. 59, no. 14, pp. 1284–1292, 2014.

[53] T. Wenzler, S. Solanki, and N. Krivova, "Reconstructed and measured total solar irradiance: Is there a secular trend between 1978 and 2003?," *Geophysical Research Letters*, vol. 36, no. 11, 2009.

About This Journal

ACC is an open access journal published by Scientific Online Publishing. This journal focus on the following scopes (but not limited to):

- Atmospheric Environment
- Climate Change and Broadcast Meteorology
- Climate Dynamics and Variability
- Climate Policy
- Atmospheric Circulation
- Aerodynamics
- Atmospheric and Oceanic Physics
- Atmospheric Chemistry
- Biometeorology and Microclimatology
- Forestry Climatology
- Clouds and Precipitation Physics
- Dynamics of Atmospheres and Ocean
- Hydrometeorology
- Navigation Climatology
- Polar Meteorology
- Weather Forecasting
- Numerical Weather Prediction
- Satellite Meteorology and Synoptic Meteorology
- Theoretical and Applied Climatology
- Hydrology, Oceans and Atmosphere

Welcome to submit your original manuscripts to us. For more information, please visit our website: http://www.scipublish.com/journals/ACC/

You can click the bellows to follow us:

- Facebook: https://www.facebook.com/scipublish
- Twitter: https://twitter.com/scionlinepub
- LinkedIn: https://www.linkedin.com/company/scientific-online-publishing-usa
- Google+: https://google.com/+ScipublishSOP

SOP welcomes authors to contribute their research outcomes under the following rules:

- Although glad to publish all original and new research achievements, SOP can't bear any misbehavior: plagiarism, forgery or manipulation of experimental data.
- As an international publisher, SOP highly values different cultures and adopts cautious attitude towards religion, politics, race, war and ethics.
- SOP helps to propagate scientific results but shares no responsibility of any legal risks or harmful effects caused by article along with the authors.
- SOP maintains the strictest peer review, but holds a neutral attitude for all the published articles.
- SOP is an open platform, waiting for senior experts serving on the editorial boards to advance the progress of research together.